Integrated Ocean Drilling Program
Expedition 340T Preliminary Report

Atlantis Massif Oceanic Core Complex

Velocity, porosity, and impedance contrasts within the domal core of Atlantis Massif: faults and hydration of lithosphere during core complex evolution

15 February–2 March 2012

Expedition 340T Scientists

Published by
Integrated Ocean Drilling Program Management International, Inc.,
for the Integrated Ocean Drilling Program

Publisher's notes

Citation:
Expedition 340T Scientists, 2012. Atlantis Massif Oceanic Core Complex: velocity, porosity, and impedance contrasts within the domal core of Atlantis Massif: faults and hydration of lithosphere during core complex evolution. *IODP Prel. Rept.,* 340T. doi:10.2204/iodp.pr.340T.2012

Distribution:
Electronic copies of this series may be obtained from the Integrated Ocean Drilling Program (IODP) Scientific Publications homepage on the World Wide Web at **www.iodp.org/scientific-publications/.**

This publication was prepared by the Integrated Ocean Drilling Program U.S. Implementing Organization (IODP-USIO): Consortium for Ocean Leadership, Lamont Doherty Earth Observatory of Columbia University, and Texas A&M University, as an account of work performed under the international Integrated Ocean Drilling Program, which is managed by IODP Management International (IODP-MI), Inc. Funding for the program is provided by the following agencies:

National Science Foundation (NSF), United States

Ministry of Education, Culture, Sports, Science and Technology (MEXT), Japan

European Consortium for Ocean Research Drilling (ECORD)

Ministry of Science and Technology (MOST), People's Republic of China

Korea Institute of Geoscience and Mineral Resources (KIGAM)

Australian Research Council (ARC) and GNS Science (New Zealand), Australian/New Zealand Consortium

Ministry of Earth Sciences (MoES), India

Disclaimer

April 2012

Expedition 340T participants

Donna Blackman
Chief Scientist
Scripps Institution of Oceanography
University of California, San Diego
9500 Gilman Drive
La Jolla CA 92093-0225
USA
dblackman@ucsd.edu

Angela L. Slagle
Expedition Project Manager/Logging Staff Scientist
Borehole Research Group
Lamont-Doherty Earth Observatory of Columbia University
PO Box 1000, 61 Route 9W
Palisades NY 10964
USA
aslagle@ldeo.columbia.edu

Gilles Guèrin
Logging Staff Scientist
Borehole Research Group
Lamont-Doherty Earth Observatory of Columbia University
PO Box 1000, 61 Route 9W
Palisades NY 10964
USA
guerin@ldeo.columbia.edu

Alistair J. Harding
Scientist
Scripps Institution of Oceanography
University of California, San Diego
9500 Gilman Drive
La Jolla CA 92093-0225
USA
aharding@ucsd.edu

Abstract

During Integrated Ocean Drilling Program (IODP) Expedition 340T we conducted borehole logging in IODP Hole U1309D on the domal core of Atlantis Massif just west of the spreading axis of the Mid-Atlantic Ridge, 30°N. Prior seismic imaging showed considerable reflectivity within the footwall of this oceanic core complex, and our new results document the geologic explanation for at least some of the impedance contrast. The dominantly gabbroic section, cored to 1415 meters below seafloor (mbsf) during IODP Expeditions 304 and 305, would not inherently contain density/seismic contrasts sufficient to reflect seismic energy. Expedition 340T aimed to test the hypothesis that highly altered intervals and/or fluid-bearing fault zones at depth might be responsible for these contrasts, thus allowing interpretation of the reflectivity patterns in terms of hydration pathways within young oceanic crust. Our results confirm that borehole velocity of altered olivine-rich troctolite intervals at Site U1309 is sufficiently distinct from surrounding rock (V_P ~0.5 km/s slower) to produce a multichannel seismic reflection given their several tens of meters thickness. Small dips in temperature (0.3°–0.5°C) were measured in borehole fluid adjacent to known faults at 750 and 1100 mbsf. These suggest that percolation of seawater along the fault zone is still active, not just a past process that produced the alteration documented in Expedition 305 core from these intervals. In addition to obtaining the first seismic coverage of the 800–1400 mbsf portion of Hole U1309D and reliable downhole temperatures, we acquired other standard logging data that are in excellent agreement with Expedition 304/305 borehole measurements. Vertical seismic profile station coverage at zero offset now extends the full length of the hole, including the uppermost 150 mbsf, where detachment processes are expected to have left their strongest imprint. Opportunistic sampling of a seafloor feature, now designated IODP Site U1392 and located a few meters from Hole U1309D, recovered fragments of possible cap rock that may provide information on processes within the exposed detachment.

Introduction

During Integrated Ocean Drilling Program (IODP) Expedition 340T we conducted borehole logging at Atlantis Massif, an oceanic core complex (OCC) just west of the spreading axis of the Mid-Atlantic Ridge, 30°N. Seismic data for the 800–1400 m interval cored in Hole U1309D during IODP Expeditions 304 and 305 are the primary new information, whereas a number of ancillary measurements at the site also aim to

address the question of where seawater penetrates and alters young oceanic lithosphere, thus hydrating a key chemical reservoir in the Earth. The detachment fault that controlled formation of Atlantis Massif (Cann et al., 1997; Blackman et al., 2002; Schroeder and John, 2004; Karson et al., 2006) is known to have localized fluid flow in a ~100 m thick zone of deformation/alteration that is exposed at the seafloor (Boschi et al., 2006; McCaig et al., 2010). Additional zones of (at least) past seawater circulation are indicated in deeper known or inferred fault zones or portions of olivine-rich troctolite intervals that are altered to serpentinite (Hirose and Hayman, 2008; Michibayashi et al., 2008; Beard et al., 2009). Seismic reflectivity observed in multichannel seismic (MCS) data throughout the Central Dome and Southern Ridge of the massif (Canales et al., 2004; Singh et al., 2004; Blackman et al., 2009) may correspond to interfaces between zones of past and/or present fluid flow and the surrounding rock. The main goal of Expedition 340T was to begin to test this hypothesis.

Background

Slow-spread ocean lithosphere accretes and evolves via temporally and spatially variable magmatic and tectonic processes (e.g., Bonatti and Honnorez, 1976; OTTER, 1984; Dick, 1989; Lin et al., 1990; Sinton and Detrick, 1992; Cannat, 1993; Lagabrielle et al., 1998). OCCs, in particular, mark significant periods (1–2 m.y.) when a distinct mode of rifting/accretion persists, in contrast to the more typical interplay between magma supply and faulting that generates the ubiquitous abyssal hills. Long-lived displacement along detachment faults active within the ~20 km wide axial zone of a slow-spreading center exhumes the characteristic domal cores of an OCC, which are often capped by spreading-parallel corrugations (e.g., Cann et al., 1997; Tucholke et al., 1998). Beneath this exposed fault zone, gabbroic rocks with lenses, or possibly greater volumes of mantle peridotite, are present, providing access to a major component of Earth's deep lithosphere for detailed chemical and physical property investigations. Conditions of OCC development are documented by igneous and metamorphic assemblages, as well as by deformation recorded during evolution of the footwall.

Geological setting

Atlantis Massif is a young OCC where regional geophysical surveys and seafloor mapping and sampling coverage are good; major structural blocks within the faulted lithosphere have been identified (Fig. **F1**). The domal core of Atlantis Massif was

unroofed via detachment faulting that occurred within the rift zone of the Mid-Atlantic Ridge at ~1.1–0.5 Ma (Blackman et al., 2011; Grimes et al., 2008). Atlantis Massif was initially hypothesized to be an OCC on the basis of morphologic and backscatter mapping and dredging results that documented the shallow, corrugated, and striated domal core underlain by mafic and ultramafic rocks (Cann et al., 1997). The spreading-parallel corrugations are equated with similar-scale features mapped on continental detachment faults (John, 1987) and suggest that the surface was a slip plane associated with the detachment fault that unroofed the dome. Schroeder and John (2004) and Karson et al. (2006) confirmed the existence of a long-lived normal fault at the top of the Southern Ridge by documenting deformation within a zone extending at least a few kilometers in length. The juxtaposition of volcanic eastern blocks against the corrugated dome, whose Southern Ridge samples include gabbroic rocks (~30%) and serpentinized peridotite (~70%), supports the OCC model. Gravity and seismic data indicate that significant portions of the footwall to the detachment contain rocks with anomalously high density (200–400 kg/m^3 greater than surrounding rock) (Blackman et al., 2008) and velocity (4–6 km/s in the upper kilometer, compared to average Atlantic upper crust at ~3–5 km/s) (Canales et al., 2008; Collins et al., 2009). The active serpentinite-hosted Lost City hydrothermal vent field (Kelley et al., 2001; Früh-Green et al., 2003) is located just below the peak of the massif at the apex of the Southern Ridge. The Central Dome, extending smoothly to the north, is several hundred meters deeper; it is against only this part of the footwall that the juxtaposed volcanic hanging wall exists. It is assumed to overlie the detachment where it extends at depth.

Differences between the Central Dome and the domal Southern Ridge (Karson et al., 2006; Boschi et al., 2006; Blackman, Ildefonse, John, Ohara, Miller, MacLeod, and the Expedition 304/305 Scientists, 2006; Blackman et al., 2011; Ildefonse et al., 2007; Canales et al., 2008) raise questions about how axial magmatism, the detachment system, and subseafloor alteration may have progressed in space and time as this core complex formed. If we can determine the geologic origin of reflectivity within the uplifted footwall to the detachment, future seismic imaging could provide definitive tests of models for along- and across-strike variation in the structure and development of oceanic core complexes. The availability of the 1415 m deep borehole at IODP Site U1309 provides a unique opportunity to groundtruth properties measured at seismic wavelengths.

Seismic studies/Site survey data

MCS data (Canales et al., 2004; Singh et al., 2004) show significant reflectivity throughout the Central Dome and Southern Ridge (Fig. **F2**), but the cause of this reflectivity is difficult to explain based on what is known about the dominantly gabbroic primary lithology at Site U1309. Results from Hole U1309D indicate that alteration varies quite rapidly downhole and there are a number of sharp changes in borehole resistivity, two of which coincide with the boundaries of several tens-of-meters thick, highly altered olivine-rich troctolite units (Fig. **F3**). The strong D-reflection, noted by Canales et al. (2004) to be pervasive throughout the dome and apparently an isolated event at 0.2–0.5 s two-way traveltime using initial processing, has been shown via a wide-angle reflection processing method (Masoomzadeh et al., 2005; Jones et al., 2007) to most likely be the first in a series of reflections (Fig. **F2**) (Singh et al., 2004). This reflective zone may be associated with altered olivine-rich troctolite units (Fig. **F2C**). However, this interpretation needs to be investigated more carefully using a better in situ velocity model and the best-possible ties to the core/borehole data.

Modeling of near-bottom explosive source (NOBEL) (Collins et al., 2009) and MCS streamer refraction traveltimes (Canales et al., 2008; Henig et al., 2010, in press) indicates that at least parts of the dome are capped by a 100–200 m thick low-velocity layer (<4 km/s) (Fig. **F2D**). Reliable first arrival times for vertical seismic profile (VSP) stations in the 50–200 m depth interval can provide groundtruth on this crucial interval, where imprints of detachment zone processes may extend beyond the very narrow, high-deformation interval documented by talc-schist fault rock sampled only in the upper several meters at Site U1309 (Blackman, Ildefonse, John, Ohara, Miller, MacLeod, and the Expedition 304/305 Scientists, 2006; Blackman et al., 2011; McCaig et al., 2010). Sonic logging in the 800–1415 meters below seafloor (mbsf) interval can provide velocity constraints on the 1080–1200 mbsf altered olivine-rich troctolite interval (Fig. **F3A**). The V_P/V_S ratio of the ~350 mbsf olivine-rich units appears to be higher (~2.0) than average (~1.8), and the Expedition 340T data can show whether this is characteristic of these units.

Scientific objectives

Two observations made during Expedition 340T inform young ocean lithosphere studies, in general. Each required minimum possible disturbance approaching and reentering the hole:

1. Visual observation of whether the well was "producing" (flow out of the hole) or not: addresses fluid flow within the crust and chemical exchange with seawater in maturing lithosphere.
2. Measurement of borehole fluid temperature: assesses conditions that may be encountered by future ultradeep drilling/logging of an intrusive oceanic section; also tests for possible fluid flow (temperature deviations) within fault zones of Atlantis Massif's footwall.

Focusing on our main objectives, obtaining new caliper measurements throughout the hole documents hole condition and guided selection of VSP station depths that might be optimum for instrument coupling. The zero-offset VSP data provide information on velocities in the vicinity of the hole at intermediate length scales and could increase our knowledge of local reflectivity for near-vertical waves, thereby improving core-log integration with surface seismic data. Information on the condition of the borehole is crucial for determining whether a future single-ship wireline reentry experiment is viable or whether the drillship and a second vessel would be needed to complete the VSP experiment by conducting a walk-away component. Ultimately, this full data set would enable core-log-survey integration at as high a level as possible with current geophysical data.

Sonic logs obtained during Expedition 340T will allow analysis of the relationship between lithology and velocity in the section deeper than 800 mbsf, where the least altered rock was recovered from Hole U1309D. In addition to compressional velocity (V_P) and shear velocity (V_S) correlations with either primary or alteration lithologies, complete hole Stoneley wave data will enable assessment of permeability/fracturing and any contrast thereof between documented fault zones and surrounding rock.

Magnetic susceptibility logs target downhole variations in magnetite that are a product of serpentinization, potentially providing constraints on extent/style of alteration that may have been missed with the finite (although very good) core recovery (nonwhite portion of Fig. **F3A**).

Downhole logging

Downhole logs are measurements of physical, chemical, and structural properties of the formation surrounding a borehole. The data are continuous with depth (at vertical sampling intervals ranging from 2.5 mm to 15 cm) and are measured in situ. The sampling is intermediate in scale between laboratory measurements on core samples and geophysical surveys and provides a necessary link for the integrated understanding of physical properties on all scales.

Logs in "hard rock" such as at Site U1309 can be interpreted in terms of the lithology, mineralogy, and geochemical composition of the penetrated formation. They also provide information on the status and size of the borehole and on possible deformations induced by drilling or formation stress. When core recovery is incomplete or disturbed, log data may provide the only way to characterize the formation. These data can be used to determine the actual thickness of individual units or lithologies when contacts are not recovered, to pinpoint the true depth of features in cores with incomplete recovery, and to identify intervals that were not recovered.

Logs are recorded with a variety of tools combined into several tool strings, which are run downhole. For deep holes, logging runs may be made to intermediate depths between coring phases to obtain wall rock measurements before multiple bit runs risk the possibility of hole degradation. Four tool strings were used during Expedition 340T in Hole U1309D, which had previously been cored and partially logged to 1415 mbsf (see Fig. **F4;** Table **T1**):

1. A modified triple combination (triple combo) tool string (gamma ray, density, resistivity, and borehole temperature),
2. A sonic string (gamma ray and sonic velocity),
3. The Versatile Seismic Imager (VSI) tool string (vertical seismic profile and gamma ray), and
4. The Magnetic Susceptibility Sonde (MSS) tool string (gamma ray, magnetic susceptibility, and temperature).

After reentering Hole U1309D, the logging bit at the end of the bottom-hole assembly (BHA) was set below the casing shoe located at ~20 mbsf, below an interval where prior experience suggested potential obstacles. Bit depth varied throughout the operations based on hole conditions. See Table **T2** for details of logging operations.

Each tool string deployment is a logging "run," starting with the assembly of the tool string and the necessary calibrations. The tool string is then sent down to the bottom of the hole while recording a partial set of data, and, except for the VSI, is pulled up at a constant speed, typically 300–500 m/h, to record the main data. The VSI is clamped against the borehole wall at regularly spaced depths while shooting the seismic source and pulled up between each station. During each run, tool strings can be lowered down and pulled up the hole several times for control of repeatability or to try to improve the quality of the data. Each lowering or hauling up of the tool string while collecting data constitutes a "pass." During each pass the incoming data are recorded and monitored in real time on the surface system. A logging run is complete once the tool string has been brought to the rig floor and disassembled.

Logged properties and tool measurement principles

The main logs recorded during Expedition 340T are listed in Table **T3.** More detailed information on individual tools and their geological applications may be found in Ellis and Singer (2007), Goldberg (1997), Lovell et al. (1998), Rider (1996), Schlumberger (1989), and Serra (1984, 1986, 1989). A complete online list of acronyms for the Schlumberger tools and measurement curves is available at **www.slb.com/modules/mnemonics/index.aspx.**

Borehole temperature

The triple combo tool string deployed during Expedition 340T included the Modular Temperature Tool (MTT) to measure the borehole fluid temperature. The MTT was designed at Lamont-Doherty Earth Observatory (LDEO) to resolve centimeter-scale temperature variations at typical logging speeds of 300–500 m/h. It uses two temperature sensors: a fast responding thermocouple and a highly accurate resistance-temperature device. The sonde also contains an accelerometer for depth correction and is combined with a specially designed cartridge to allow data transmission through the Schlumberger tool string and wireline.

Additional temperature measurements were made during each logging run by a sensor in the logging equipment head–mud temperature (LEH-MT) cablehead and processed by the Enhanced Digital Telemetry Cartridge (EDTC) (see **"Telemetry cartridges"**).

Natural radioactivity

The EDTC (see **"Telemetry cartridges"**), which is used primarily to communicate data to the surface, also includes a sodium iodide scintillation detector to measure the total natural gamma ray emission. It is not a spectral tool but it provides high-resolution total gamma ray for each pass that allows for precise depth-match processing between logging runs and passes.

Density

Formation density was measured with the Hostile Environment Litho-Density Sonde (HLDS). The sonde contains a radioactive cesium (^{137}Cs) gamma ray source (622 keV) and far and near gamma ray detectors mounted on a shielded skid, which is pressed against the borehole wall by an eccentralizing arm. Gamma rays emitted by the source undergo Compton scattering, whereby gamma rays are scattered by electrons in the formation. The number of scattered gamma rays that reach the detectors is proportional to the density of electrons in the formation, which is in turn related to bulk density. Porosity may also be derived from this bulk density if the matrix (grain) density is known. Good contact between the tool and borehole wall is essential for good HLDS logs; poor contact results in underestimation of density values.

The HLDS also measures photoelectric absorption as the photoelectric effect (PEF). Photoelectric absorption of the gamma rays occurs when their energy is reduced below 150 keV after being repeatedly scattered by electrons in the formation. Because PEF depends on the atomic number of the elements encountered, it varies with the chemical composition of the minerals present and can be used for the identification of some minerals (Bartetzko et al., 2003; Blackman, Ildefonse, John, Ohara, Miller, MacLeod, and the Expedition 304/305 Scientists, 2006).

Electrical resistivity

The High-Resolution Laterolog Array (HRLA) tool provides six resistivity measurements with different depths of investigation (including the borehole fluid, or mud, resistivity and five measurements of formation resistivity with increasing penetration into the formation). The sonde sends a focused current beam into the formation and measures the intensity necessary to maintain a constant drop in voltage across a fixed interval, providing direct resistivity measurement. The array has one central (source) electrode and six electrodes above and below it, which serve alternately as focusing and returning current electrodes. By rapidly changing the role of these electrodes, a simultaneous resistivity measurement at six penetration depths is achieved. The tool

is designed to ensure that all signals are measured at exactly the same time and same tool position, and to reduce the sensitivity to shoulder bed effects. The design, which eliminates the need for a surface reference electrode, improves formation resistivity evaluation compared to the traditional dual laterolog sonde that was used in previous expeditions to Hole U1309D.

Typically, igneous minerals found in crustal rocks are electrical insulators, whereas sulfide and oxide minerals as well as ionic solutions like pore water are conductors. In most rocks, electrical conduction occurs primarily by ion transport through pore fluids and, thus, is strongly dependent on porosity. Electrical resistivity can hence be used to estimate porosity, alteration, and fluid salinity.

Acoustic velocity

The Dipole Sonic Imager (DSI) generates acoustic pulses from various sonic transmitters and records the full waveforms with an array of eight receivers. The waveforms are then used to calculate the sonic velocity in the formation. The omnidirectional monopole transmitter emits high-frequency (5–15 kHz) pulses to extract the compressional velocity (V_P) of the formation, as well as the shear velocity (V_S) when it is faster than the sound velocity in the borehole fluid. The same transmitter can be fired in sequence at a lower frequency (0.5–1 kHz) to generate Stoneley waves that are sensitive to fractures and variations in permeability. The DSI also has two dipole transmitters, which allow an additional measurement of shear wave velocity in "slow" formations, where V_S is slower than the velocity in the borehole fluid. However, in formations such as the basement penetrated in Hole U1309D, V_S was primarily measured from the monopole waveforms. These higher frequency waveforms usually provide a sharper shear arrival and more accurate estimate of V_S than either of the dipole sources. The two shear velocities measured from the two orthogonal dipole transducers can be used to identify sonic anisotropy that can be associated with the local stress regime.

During acquisition, V_P and V_S are extracted from the recorded waveforms using a slowness/time coherence processing algorithm (Kimball and Marzetta, 1984). In the process, a semblance function is calculated for a fixed time window across the receiver array, varying traveltimes and velocity within a predefined range to identify peaks in semblance corresponding to individual mode arrivals. Acquisition parameters were configured for the velocity range expected in the deepest part of Hole U1309D (V_P = 6–7 km/s).

Accelerometry and magnetic field measurement

The traditional purpose of the General Purpose Inclinometry Tool (GPIT), which includes a three-component accelerometer and a three-component magnetometer, is to determine the acceleration and orientation of the imaging tools. During Expedition 340T, the GPIT was used primarily to provide orientation for the cross-dipole data from the DSI.

Vertical seismic profile

In a VSP experiment, a borehole seismic tool is anchored against the borehole wall at regularly spaced intervals and records the acoustic waves generated by a seismic source positioned just below the sea surface. The first purpose of these measurements is to provide a direct measurement of the time necessary for seismic waves to travel from the surface to a given depth, to tie the observations in the well, recorded as a function of depth, to the reflections observed in the seismic survey data, recorded as a function of time. In addition, analysis of the full waveforms can be used to characterize seismic reflectivity beyond the borehole, which could help document the structure within Atlantis Massif core complex.

The seismic source for the VSP was a Sercel G-gun parallel cluster, composed of two 250 in^3 air guns separated by 1 m. It was positioned by one of the ship cranes on the port side of the ship at distance of 27.4 m from the centerline of the ship. The setback along the centerline from the top of the wellhead was 35.5 m, and the total horizontal (diagonal) offset from the wellhead was 44.7 m. The air guns were suspended from a float at a water depth of ~7 m, corresponding to a notch frequency of 107 Hz. The average firing pressure was 1950 psi but noted as varying by up to ±50 psi over the course of operations. Minimum firing interval during VSP operations was 18 s, and pressure recovery after firing was ~5 s, so shot-to-shot variations in pressure were minimal. The bubble pulse interval was ~125 ms.

During operation, dynamic positioning (DP) maintained the wellhead over Hole U1309D, but the ship's heading was changed between the 2 days of VSP operation from 335° on the first day to 040° on the second. This is significant because the slope of the seafloor is ~11°, shoaling most rapidly in a southwest direction. These headings placed the gun array on the updip side of Hole U1309D and increased the chances of recording nonvertical ray paths and polarizations at intermediate depths.

In accordance with the requirements of the National Environmental Policy Act (NEPA) and of the Endangered Species Act, all seismic activities were conducted during daytime and protected species observers (PSOs) kept watch for protected species during the entire duration of the zero-offset VSP. Any sight of protected species within the exclusion zone of 940 m (defined for water depths > 1000 m) would interrupt the survey for 60 min after the last sighting or until the protected species were seen leaving the exclusion zone. PSOs began observations 1 h prior to the use of the seismic source, which started with a 30 min ramp-up procedure, gradually increasing the operational pressure and firing rate to provide time for undetected protected species to vacate the area. The same ramp-up procedure would be used when resuming activity after any interruption due to the sighting of protected species or whenever the gun was not fired for more than 30 min.

The seismometer used was the VSI sensor, a three-axis geophone accelerometer, that was anchored against the borehole prior to recording by a caliper arm. The orientation of the horizontal components, *x* and *y*, varies due to sensor rotation during logging, but relative tool orientation during the run is recorded. Data were recorded in three sessions over 2 days. The first session was ended and the tool string recovered when it was determined that the VSI was no longer clamping due to a broken caliper. Recording conditions were very good for the second deployment, and the session ended only because of fading daylight. In contrast, conditions were extremely noisy the following day. The replacement caliper became slightly bent during operations, but noisy conditions were evident from the beginning of recording and persisted during the day; the reason is undiagnosed.

Data were recorded at 55 station depths between 1645 and 3005 meters below sea level (mbsl), or 0 and 1360 mbsf, corresponding to an average station spacing of 25 m. Stations at 2705, 2955, 2979, and 3005 mbsl were repeated due to failure of the caliper on the first deployment. Stations deeper than 3005 mbsl were not attempted as a precaution against damage to the instrument. A total of 659 shots were recorded; between 5 and 32 recordings were taken at each station with a median of 10.

VSP data format description

The data from the experiment are available in SEGY format for the individual shots as *x*-, *y*-, and *z*-components, the shot break hydrophone, and the automatic stack of traces produced during logging for individual stations. There are 659 traces in both raw data files and in the shot break file, although shot numbers, the third long integer entry in the SEGY header (i.e., 3L), ranges from 3 to 680 with some intermediate shots

not recorded. Some unrecorded shots were fired manually between stations to maintain compliance with NEPA. The stacked files have 60 traces rather than 55 because the 4 repeated stations at 2705, 2955, 2979, and 3005 mbsl appear twice, and the station at 1795 mbsl appears twice, as it was reclamped during shooting.

Trace data are recorded in Institute of Electrical and Electronics Engineers (IEEE) floating point format with raw data amplitudes reaching almost 900 due to the noise; maximum signal amplitudes are typically <1. Start times for the raw traces are the source trigger times uncorrected for the source delay, which can be derived from the shot break records. Recorded maximum shot break amplitudes diminish around Shot 148, possibly due to slight misalignment of the guns; there was no indication of gun malfunction during operations.

The datum for elevation is the drill rig floor and the receiver group elevation with respect to sea level (Header 11L) is derived from the downhole depth (Header 14L) using a standard 11 m correction for rig floor. Estimates of the ship's draft during the VSP put actual elevation of the rig floor at 11.5 m.

Magnetic Susceptibility Sonde

The MSS, a wireline tool designed by LDEO, measures the ease with which formations are magnetized when subjected to Earth's magnetic field. The ease of magnetization is ultimately related to the concentration and composition (size, shape, and mineralogy) of magnetizable material within the formation. These measurements provide one of the best methods for investigating stratigraphic changes in mineralogy and lithology because the measurement is quick, repeatable, and nondestructive and because different lithologies often have strongly contrasting susceptibilities. The sensor used during Expedition 340T was a dual-coil sensor providing deeper reading measurements with a vertical resolution of ~40 cm. The MSS was run as a component of a Schlumberger tool string, using a specially developed data translation cartridge, saving hours of operation time. For quality control and environmental correction, the MSS also measures internal tool temperature, *z*-axis acceleration, and low-resolution borehole conductivity.

The MSS used during Expedition 340T was run for the first time in seawater in Hole U1309D. Core sample data available from Expeditions 304/305 provide a means to test operational sensitivities of the deep-reading sensor as well as an opportunity to obtain constraints on absolute calibration parameters for the tool.

Auxiliary logging equipment

Cable head

The Schlumberger logging equipment head (LEH), or cablehead, measures tension at the very top of the wireline tool string, which diagnoses difficulties in running the tool string up or down the borehole, or when exiting or entering the drill string or casing. The LEH-MT used during Expedition 340T also includes a thermal probe to measure the borehole fluid temperature. Several of the Expedition 340T runs encountered difficulty as the tool strings passed out of, or in to, the BHA, as documented by the LEH.

Telemetry cartridges

Telemetry cartridges are used in each tool string to allow the transmission of the data from the tools to the surface. The EDTC also includes a sodium iodide scintillation detector to measure the total natural gamma ray emission of the formation. This gamma ray log was used to match the depths between the different passes and runs. In addition, it includes an accelerometer, whose data can be used in real time to evaluate the efficiency of the wireline heave compensator (WHC). The temperature measurements from the LEH-MT are also processed by the EDTC before being sent to the surface for real-time monitoring.

Joints and adapters

Because the tool strings combine tools of different generations and with various designs, they include several adapters and joints between individual tools to allow communication, provide isolation, avoid interferences (mechanical and acoustic), terminate wirings, or to position the tool properly in the borehole. The knuckle joints in particular were used to allow some of the tools such as the HRLA to remain centralized in the borehole, while the overlying HLDS was simultaneously pressed against the borehole wall by an eccentralizing arm.

All these additions contribute to the total length of the tool strings and are included in Figure **F4.**

Log data quality

A principal factor in the quality of log data is the condition of the borehole wall. If the borehole diameter varies over short intervals because of washouts or ledges, the

logs from tools that require good contact with the borehole wall (i.e., density tool in the Expedition 340T program) may be degraded. Deep investigation measurements such as gamma ray, resistivity, and sonic velocity, which do not require contact with the borehole wall, are generally less sensitive to borehole conditions. Very narrow ("bridged") sections will also cause irregular log results. For the VSI, cable motion and/or ship noise can also be an important factor controlling data quality.

The quality of the logging depth determination depends on several factors. The depth of the logging measurements is determined from the length of the cable played out from the winch on the ship. Uncertainties in the depth of the core samples occur because of incomplete core recovery or incomplete heave compensation. Uncertainties in logging depth occur because of ship heave, cable stretch, cable slip, or even tidal changes. All these factors generate some discrepancy between core sample depths, logs, and individual logging passes. To minimize the effect of ship heave, a hydraulic wireline heave compensator is used to adjust the wireline length for rig motion during wireline logging operations.

Wireline heave compensator

Expedition 340T continued to evaluate the WHC system. It is designed to compensate for the vertical motion of the ship and maintain steady motion of the logging tools downhole. It uses vertical acceleration measurements made by a motion reference unit (MRU), located under the rig floor near the center of gravity of the ship, to calculate the vertical motion of the ship. It then adjusts the length of the wireline by varying the distance between two sets of pulleys through which the cable passes. Real-time measurements of uphole (surface) and downhole acceleration are made simultaneously by the MRU and by the EDTC tool, respectively. An LDEO-developed software package allows these data to be analyzed and compared in real time, displaying the actual motion of the logging tool string, and enabling evaluation of the efficiency of the compensator. Observations during Expedition 340T neither confirm nor disprove the effectiveness of this system. The best signal-to-noise ratio VSI recordings were obtained when the WHC was turned off and stations were relatively shallow (shallower than 1810 meters below rig floor [mbrf] [150 mbsf]). However, sea conditions on a subsequent run when signal-to-noise ratio was poor and the WHC was in use were somewhat different so interpretation of the difference is difficult. Three stations recorded with the WHC off during that run did not result in a recognizable difference in noise levels on the VSI trace.

Logging data flow and processing

Data for each wireline logging run were monitored in real time and recorded using the Schlumberger MAXIS 500 system. They were then copied to the shipboard processing stations for preliminary processing. Each pass was depth matched to logs from Expeditions 304 and 305. After depth-match processing, all the logging depths were shifted to the seafloor. This is usually done by identifying the seafloor from a step in gamma radiation, but in this case the logs were shifted using the depth to seafloor established from previous expeditions to Hole U1309D. These data were made available to the science party within a day after their acquisition.

The downhole log data were also transferred onshore to LDEO for standardized data processing. The main part of the processing is depth matching to remove depth offsets between different logging passes, which results in a new depth scale: wireline matched depth below seafloor (WMSF). Also, additional corrections are made to certain tools and logs (e.g., speed and voltage corrections to resistivity images), documentation for the logs (with an assessment of log quality) is prepared, and the data are converted to ASCII for the conventional logs and to SEGY for the VSP data. Schlumberger GeoQuest's GeoFrame software package is used for most of the processing.

Operations summary

The vessel arrived on location at 2230 h on 20 February 2012 after making a rapid passage from Lisbon, Portugal, with an average transit speed of 12.37 kt over the 1713 nmi distance. The R/V *JOIDES Resolution*'s excellent transit speed can most likely be attributed to a recently cleaned hull, newly polished propellers, and favorable winds and seas. During the transit to the first site, the drilling and logging equipment was inspected and tested to ensure performance during Expedition 340T operations. Prior to the start of logging operations, a presite meeting was held with Siem Offshore staff, IODP staff, the Chief Scientist, and other critical staff.

On arrival at Site U1309, the speed of the vessel was reduced and bridge control was shifted to DP control at 2257 h. Drill floor operations began immediately after switching to DP control. First, the upper guide horn was laid out, the BHA for logging operations was picked up and assembled, and the drilling string was run to the seafloor. Despite preoperational checks, the iron roughneck torquing system failed during the initial pipe trip. While troubleshooting the hydraulic problem, tripping continued us-

ing manual tongs and a rope to spin in the drill pipe. The vibration-isolated television (VIT) frame was installed while tripping to the bottom, and at 1015 h on 21 February we began spacing out the bit for reentry into Hole U1309D. What appeared to be the reentry cone was identified almost immediately, and the vessel was positioned for a reentry at ~1115 h. The reentry attempt was made but was unsuccessful, primarily because the assumed reentry cone was in fact a conelike seafloor structure. A bottom survey was then conducted to locate the Hole U1309D reentry cone. It was located and reentered at 1320 h on 21 February. After reentry the logging bit was positioned at 1711 mbrf, which is below known problem sections in Hole U1309D.

The triple combo tool string was rigged up by 1440 h on 21 February and lowered to the hole. The tool string was run into the hole, recording standard measurements as well as an in situ temperature profile from the surface to 3060 mbrf. At 0050 h on 22 February, the tool string was completely back in the pipe but unable to pass through the BHA. After working the logging string for >4 h, the decision was made to use the Kinley crimper/cutter to crimp and cut the logging cable. After deploying two crimping systems and a cutter, the cable was cut and retrieved. The VIT frame was then run to the seabed to verify that the tools were present at the end of the bit. The drill bit cleared the reentry cone at 1410 h. The bottom of the logging tool string was visually observed hanging out of the end of the bit. The drill string was then pulled to surface and a stand of the BHA was set back. The logging tools were removed from the last drill collar with care. All tools were successfully recovered including the radioactive source. It was immediately apparent that both centralizers had failed. The center section of the centralizers appears to have been severely abraded by the formation, likely breaking during pipe reentry. After rigging down the logging tools, the drill string was tripped back into the hole. The VIT frame was then deployed but had to be retrieved for repairs after one of the lights failed. On redeployment the lighting system failed again. The VIT frame was again pulled back and an electronics pod was changed. At 0515 h on 23 February, the VIT frame was again installed and then run to bottom. The vessel was positioned for reentry into Hole U1309D, which occurred at 0705 h. The drill string was run into the hole to 1711 mbrf. The VIT frame was retrieved.

A protected species watch was initiated at 0630 h on 23 February, and the seismic source (a G-gun parallel cluster of two 250 in^3 air guns) was deployed 7 mbsl, in preparation for a VSP experiment. After 1 h with no protected species sightings, the seismic guns were soft-started and ramped up to full pressure over the course of the next 30 min. The guns then remained on standby but were fired at least once every 30 min until the VSP experiment began. The VSI tool string was rigged up at 0815 h and run

into the hole. The first seismic station was established at 1805 mbrf, and the first shot of the VSP was fired. After a successful first station, the tool string was run to the bottom of the hole to the deepest station at 3016 mbrf. At 3016 mbrf and four successively shallower stations, data indicated that the VSI was not clamping properly. After a period of troubleshooting, the tool was pulled back to surface, where it was confirmed that the caliper was broken. A second VSI sonde was substituted into the tool string, and it was run back into the hole for 1 h of logging before sunset. Three stations were completed, and VSP operations ended for the day because of darkness. The VSI tool string was pulled back to surface and rigged down by 1910 h.

The DSI (sonic) tool string was run next. Given that it used the same centralizers as the triple combo, a decision was made to only log the deep portion of the hole that had not been logged during Expedition 305. The logging bit was tripped down to 2356 mbrf, or 700 mbsf. The pipe trip identified further ledges at 1723, 1726, and 1740 mbrf. The passive heave compensator had to be opened up to pass these ledges. At 2200 h, the DSI tool string was rigged up and run into the hole. The tool string started taking weight inside the BHA and could not be run down to the depth of the drill bit. After unsuccessfully working the tool string for 1 h to pass the BHA, the tool string was pulled back to surface and rigged down at 0330 h on 24 February. Initially there was a concern that something was either damaged or obstructing the BHA. An extended core barrel (XCB) was rigged up and run on wireline to verify that the BHA was free and clear to the bit. After verifying that the BHA was clear, the investigation turned to the DSI tool string. An obstruction was identified at one of the centralizers. The centralizers were cleaned of all rubberized backing material, and this allowed the sonic tool string to clear the landing seat.

While the centralizers were being fixed, the VSI tool string was rigged up and run into the hole to begin the second day of the VSP experiment. The protected species watch began again at 0630 h, and the G-gun cluster was deployed and ramped up following the same method as the previous day. The VSI tool string was run into the hole at 0725 h on 24 February. The VSP experiment continued through the day and was completed prior to dusk. The tool string was then pulled to the surface and rigged down. The logging bit was tripped to 2356 mbrf, or 700 mbsf past the identified ledges at 1723, 1726, and 1740 mbrf. Again, the passive heave compensator had to be opened up to pass these ledges.

At 2020 h, the DSI tool string was rigged up for a second deployment. The tool string was successfully run through the BHA to 3040 mbrf and back up to the surface with

no difficulties. The logging run was concluded at 0435 h on 25 February, when the tools were rigged down on the drill floor.

The drill pipe was tripped back to 1759 mbrf so that the upper portion of the hole could be logged with the MSS tool string, which was the final logging run in Hole U1309D. The MSS tool is temperature-limited to 80°C, so the tool string was run into the hole and recorded data from a maximum depth of 2419 mbrf up to the drill pipe. The tool string was run back down, and a repeat pass was recorded from 2165 mbrf up to the surface. By 1030 h, the tools were back on the surface and rigged down. The drill string was pulled clear of the reentry cone at 1055 h and spaced out for a bottom survey.

A seafloor survey was started from Hole U1309D by moving 5 m east, then 5 m south, and then 10 m west in an expanding spiral. The survey was concluded after 1.5 h. An attempt was made to retrieve a sample from a moundlike feature on the seafloor at 30°10.1179′N, 042°07.1118′W. The bit was set down inside the conelike opening of the feature, and a modified advanced piston core (APC) core barrel was lowered by wireline and run into the bottom twice to attempt to sample the material inside the feature. After IODP Hole U1392A was spudded at 1447 h, the core barrel was retrieved and laid out on the drill floor, and the sample was extracted for processing by the technical staff. The drilling string was then pulled back to the drill floor, and the drill collars were secured in the their racks, the upper guide horn was reinstalled, and the rig floor was secured for transit at 2030 h. The thrusters were then raised, and a magnetometer survey was started. The expedition ended with the *JOIDES Resolution* running two crossing lines with the magnetometer above Site U1309 and preparing to get under way to San Juan, Puerto Rico.

Principal results

Measurements of borehole properties form the majority of Expedition 340T results. VSP data extend the new information out to a region including a few hundred meters distance from the 1415 mbsf deep hole at Site U1309. In addition to logging in Hole U1309D, observations of the nearby seafloor were made with the VIT camera. One previously unrecognized feature generated sufficient interest that a brief sampling effort was made there. A small amount of material was successfully recovered, and the location was designated Site U1392. A map of these IODP sites on the Central Dome

of Atlantis Massif shows the spatial relationship between Expedition 304/305 Holes U1309A–U1309E and Expedition 340T Hole U1392A (Fig. F5).

Site U1309

All components of the planned logging program in Hole U1309D were successfully conducted during Expedition 340T. The triple combo, sonic, and magnetic susceptibility runs produced high-quality data. The majority of the VSP data are noisy and will require substantial postprocessing. However, a few stations in the upper 150 m of the section recorded clear, strong seismic arrivals, thus providing in situ constraints on average properties across the zone inferred to be most strongly affected by detachment processes at the Central Dome. The details and timing of logging operations in Hole U1309D are given in Table T2.

The reentry cone for Hole U1309D was approached slowly as the ship positioned to get the logging bit into the borehole. Several observers carefully watched the VIT video for indication of possible seawater flow from the opening, but none was seen, so reentry proceeded without delay.

Data quality

The main logs recorded by the triple combo, sonic, and magnetic susceptibility tool strings in Hole U1309D are displayed in Figures F6, F7, and F8. Borehole size and shape measured by the calipers are general indicators of data quality. Hole U1309D is larger and more irregular in the upper 750 m, where borehole diameter ranges from ~11 to 18 inches, whereas the lower ~650 m is generally more regular in shape with a diameter closer to bit size (Fig. F6). Anomalously low density values in the wider, irregular sections of the hole are a consequence of the inability of the tool sensors to make full contact with the borehole wall. The gamma ray and deep resistivity measurements should not be affected by the size of the borehole.

The clear arrivals in the monopole waveforms and the high coherence in the compressional and shear velocity tracks shown in Figure F7 indicate that the DSI was able to measure reliable velocity values.

Magnetic susceptibility, measured with the deep-reading sensor of the MSS, should be fairly insensitive to standoff from the borehole wall. The MSS is a relatively new logging tool that was not available during Expedition 304/305; however, the reliability of the magnetic susceptibility log can be assessed by comparison with measurements

made on Expedition 304/305 core pieces with the multisensor track (MST) system. Figure F8 shows good agreement between the two data sets, tracking meter-scale high-amplitude features at the same depths. MSS data are not yet calibrated for temperature, and the offset between the down, main, and repeat passes is most likely due to the variation in internal tool temperature between the runs (see temperature track, Fig. F8).

The comparison between hole size from Expeditions 304/305 and 340T in Figure F9 shows that the hole has not changed appreciably in the 7 y since it was last occupied. Intervals with a rough, irregular shape are indicated in the same areas, and distinct features are clearly repeated between the data sets. During the triple combo deployment of Expedition 340T, the caliper measured hole diameter to be <6 inches between 1387 and 1404 mbsf, suggesting that the lower ~20 m of the hole may contain some fall-in material. The small-diameter interval recorded between 630 and 655 mbsf in Expedition 305 data was due to tool failure and should not be interpreted as the hole having changed in diameter. Gamma radiation, density, resistivity, and sonic velocity data show good repeatability between the three sets of logs where coverage overlaps.

Scientific results

A steady increase in borehole fluid temperature with depth was documented, and a value of 146.2°C was recorded at 1405 mbsf (Fig. F10). This is >20°C hotter than the maximum temperature recorded in the hole at the end Expedition 305, when drilling and flushing had altered conditions considerably. The present temperature profile is quasilinear as a simple conductive model would predict for equilibrium conditions, but modest deviations do exist, as discussed in **"Discussion."** The few-degree dips in temperature observed in the Expedition 305 Temperature/Acceleration/Pressure data (black curve, Fig. F10) are not apparent in the 340T data until the dominant linear trend is removed; then dips of a fraction of a degree Celsius are visible near 1100 and ~750 mbsf.

The Expedition 340T VSP data are noisy enough that the automated stack computed during acquisition produced only a few reasonable quality traces. A preliminary assessment was made of the quality for individual shots using a 10–60 Hz band-pass filter and a sliding short time window centered on the predicted arrival time (see **"Appendix"**). Arrival time predictions were generated from vertical integration of the sonic log data and also one-dimensional velocity modeling for the hole taken from a 3-D tomography model of Atlantis Massif developed from surface MCS data (Henig et al., in press) (Fig. F11). The maximum difference in predicted arrival times from these

two models is 8 ms. Predicted times were adjusted for the gun firing delay (~28 ms), gun depth (5 ms), and a predicted time advance due to the sloping seafloor (~13 ms). First arrivals from 93 out of the 659 shots, corresponding to 33 of the 55 station depths, were graded as excellent to very good on at least one channel, primarily the vertical component (Tables **T4, T5**). Although necessarily subjective, an arrival was graded as excellent (value of 4 in Table **T4**) if the trace was quiet before the first break and a reliable traveltime could be picked directly from the trace. A "very good" arrival (value of 3 in Table **T4**) was one for which a reliable traveltime is expected to be obtainable by stacking and/or waveform cross-correlation. The good VSP stations for Expedition 340T thus range from 86 to 1360 mbsf, extending coverage beyond the Expedition 305 data interval of 272–792 mbsf (Collins et al., 2009). An example of excellent quality data on all three components is displayed in Figure **F12** for the new station at 150 mbsf. If relative station amplitudes are reliable, these traces indicate that the first arrival arrives with direction ~30° from the vertical. The single good arrival for the deepest station at 1360 mbsf is displayed in Figure **F13,** arriving just before the model prediction.

The most significant new data are the sonic logs recorded below 820 mbsf where no velocities were measured at the end of Expedition 305. These data are the first in situ measurements of the velocity of gabbros typical of oceanic lower crust, with V_P reaching values > 7000 m/s. V_P and V_S show little variation in the main gabbroic zone between ~760 and ~1070 mbsf, reflecting the mostly uniform composition in this zone (Blackman, Ildefonse, John, Ohara, Miller, MacLeod, and the Expedition 304/305 Scientists, 2006). Deeper in the hole, velocity seems to reflect the variation in composition, with high variability in the olivine-rich troctolite interval between 1070 and 1230 mbsf and steady values below this depth where gabbros are again dominant (Fig. **F7**).

In addition to the high-frequency (~12 kHz) waveforms used for the velocity logs, the same transducers were used to generate low-frequency (~500 Hz) Stoneley waveforms that can be used to identify fractures or permeable intervals. When they encounter fractures, Stoneley waves propagating in the borehole are reflected, with the reflectivity dependent on the openness and permeability of the fracture (Hornby et al., 1989). The chevron-shaped patterns that can be seen at various depths in the Stoneley waveforms in Figure **F7** are generated by such fracture-induced reflectivity. Figure **F14** shows that the fracture responsible for these patterns around 1345 mbsf is a 30 cm thick northeast-dipping fracture that is clearly identified in the Formation MicroScanner (FMS) images recorded during Expedition 305 logging operations.

This expedition marked the first sea trial of the deep-reading sensor of the newly rebuilt LDEO MSS. Figure **F15** shows finer scale variations of core and log susceptibility with lithology from Blackman, Ildefonse, John, Ohara, Miller, MacLeod, and the Expedition 304/305 Scientists (2006) between 170 and 400 mbsf. The background gabbroic rocks in Hole U1309D have relatively low susceptibility, whereas highest values (or highest amplitude features) are associated with intervals of oxide gabbro and highly serpentinized ultramafic rocks (e.g., olivine-rich troctolite, dunite, and harzburgite). There is a very good correlation between the magnetic susceptibility logs and the lithologies that have a high content of ferro- and ferrimagnetic minerals.

Site U1392

A seafloor feature located 3 m south and 2 m east of the reentry cone for Hole U1309D caught our interest during Expedition 340T. It was first seen shortly after the seafloor came into view on the VIT camera, as the positioning for reentry was starting. The circular shape of the feature and distinct coloring relative to surrounding seafloor gave the impression that it was the (still distant) reentry cone, so we dynamic positioned to it. Additional characteristics became evident with closer view (Fig. **F16**). A distinct rim separates the center of the feature from surrounding material. Outside the rim, concentric or stacked intervals are distinguishable from the observed shadow pattern. Inside the rim, partial darker shadow is suggestive of an opening, but otherwise the imagery there lacks structure as might be typical for unconsolidated sediment. The VIT imagery is not high quality, but these characteristics were clearly and repeatedly observed at the feature, being more evident in video than in single frames. This feature was named Decoy mound due to our initial misinterpretation that it was the reentry cone for Hole U1309D with sediment encrusted on/around/below it.

The ~2 m diameter, 1–2 m high Decoy mound was initially interpreted as a deposit formed since IODP was last at Site U1309 (February 2005). Its solid, possibly cylindrical wall, of thickness comparable to the diameter of the drill bit (~25 cm), has outside morphology that is characteristic of geothermal deposition: rounded or bulbous layers that vary in thickness (distance?) from the main rim diameter. The rim (top of the wall?) has somewhat irregular shape but is clearly distinct from the interior material. The height of the feature varies around its circumference. The logging bit could only penetrate 1–2 m below the rim before encountering a solid interface that could not be pushed through. It is this interface that was sampled as Hole U1392A.

The motivation for sampling was to test the inference that Decoy mound included (or was solely) geothermal deposits, whose composition might provide insight into any fluids responsible for the growth or, perhaps, simply lithification of preexisting or concurrently deposited sediments. The fact that the actual reentry cone for Hole U1309D was relatively sediment free (Fig. **F16**) indicates that background marine deposition since 2005 has not been significant.

There was not sufficient time after the primary work of Expedition 340T (logging) to run pipe, change the logging bit to an APC bit, and return to the seafloor for a sample, so an alternate strategy was devised. A modified APC bit was lowered in the pipe to 1500 mbrf and held there while the ship was positioned over Decoy mound. The drill string was pushed into contact with the impenetrable surface below the rim and held there. The cable tension was freed, allowing the barrel to obtain a gravity core, with intent that the flapper valve could retain material penetrated. Cable was reeled in to position the barrel again near 1500 mbrf and then tension released for a repeat sampling attempt. The core barrel was recovered after this second drop. The core catcher contained a small amount of material that was catalogued as Sample 340T-U1392A-1M-CC, the "M" indicating miscellaneous sample type.

Core 340T-U1392A-1M contained ~17 g of mixed rock fragments and some microfossils (Fig. **F17A**). Four types of material were recognized during visual inspection by nonexpert geoscientists onboard. About a third of the sample consists of sharp-edged, platy fragments (Fig. **F17B**) that are black on one side when wet and rust-colored on the other side. The black side is commonly finely striated. A few angular grains of possible fault rock are milky or translucent and white-blue in color (Fig. **F17C**), reminiscent of the talc-tremolite schist obtained in prior Atlantis Massif studies (Boschi et al., 2006; Blackman, Ildefonse, John, Ohara, Miller, MacLeod, and the Expedition 304/305 Scientists, 2006). Lithified carbonate pebbles also make up a few percent of the sample, and these pieces incorporate a variety of other material as tiny grains (Fig. **F17D**). The majority of the sample consists of dark green-gray angular subcentimeter-sized fragments (Fig. **F17E**) mixed with tiny grains of the previously described rock chip types. Microfossils also were obtained in this sample, as can be seen in this image.

Discussion

Preliminary findings for Expedition 340T fall into the following categories: (1) seismic structure of the intrusive crust within the domal core of Atlantis Massif and correlation of meter-scale velocity with general lithology, alteration, and fault zones; (2) inferences about localized fluid flow and deformation at the site based on seafloor imagery and downhole temperature; and (3) magnetic susceptibility of the borehole rock and potential for insights on relative timing of serpentinization. Most results were obtained by logging Hole U1309D, but brief camera surveys and opportunistic sampling in the new Hole U1392A added to our findings.

We have obtained the first in situ measurement of intrusive oceanic crust, which typically comprises seismic Layer 3. The Expedition 340T sonic logs indicate that the little-altered section from 800 to 1400 mbsf has mean compressional velocity of 6.6 km/s and mean shear velocity of 3.7 km/s (Fig. **F18**). This average excludes the olivine-rich troctolite interval at 1070–1220 mbsf that has several highly serpentinized intervals. The multimeter-scale sonic log average is an appropriate value for the inherent seismic properties of a gabbroic section. When postprocessing of the VSP data is complete, we will obtain a site average V_P for this intrusive crustal section that will include any effects of fracturing at the 100 m scale such as may be associated with OCC development.

Useful VSP stations bracket the range of lithologies and alteration that occur in Hole U1309D (Fig. **F19**). Only a single station from Expedition 305 is located in the interval above the upper olivine-rich troctolites (310–350 mbsf) but well below the diabase units that are common in the upper 130 mbsf.

The Expedition 340T sonic log confirms that olivine-rich troctolite intervals have sufficient velocity contrast with surrounding rock to be responsible for reflectivity observed in surface seismic data (Fig. **F18**). The 750 mbsf fault zone also has significant seismic and density contrast, but its 20–30 m thickness is at the margin of observability, relative to subseafloor seismic wavelengths. However, if pore fluid presently exists there, as suggested by the temperature dip measured in this zone (Fig. **F20A**), this could enhance the impedance contrast and produce a reflector despite the narrow interval. An additional reflector occurs at 1340 mbsf, as is most easily seen in the Stoneley wave results (Fig. **F7**). This is the first recognition of this zone as having distinctive properties—Expedition 304/305 core/logging analyses did not highlight this interval,

but a retrospective review of FMS, borehole density, porosity, and photoelectric data does show it as a distinctive, narrow interval.

Small deviations from a downhole conductive thermal gradient provide another indication that narrow depth intervals within the domal core of Atlantis Massif have distinctive properties, and, likely, currently active processes. In addition to the temperature dip associated with the 750 mbsf fault zone mentioned above, a similar small dip (0.3°–0.5°C, relative to the local linear gradient) is observed at the 1100 mbsf fault zone (Fig. **F20**). Our preliminary interpretation of these signals is that slow percolation of seawater (cooler temperature [*T*] when it initially enters a fracture network at the seafloor, whether at or laterally displaced from Site U1309) occurs, made possible by modest porosity within these zones. The maximum vertical extent of each zone is 10–20 m based on the limit of the *T* deviation. Michibayashi et al. (2008) determine a ~6 m thickness for the fault zone at 750 mbsf on the basis of borehole resistivity, gamma ray, and density anomalies. Borehole structure imaged in Expedition 304/305 FMS data tends to dip east in a central 1 m interval of this zone, in contrast to the general north–south dip of the structures above and below. Low resistivity and positive gamma ray and neutron porosity signatures in the fault zone are consistent with the presence of a conductive phase such as seawater.

The downhole temperature profile has 2–3 modest breaks in slope; characterizing their location and investigating potential reasons for the changes in gradient will be addressed in postcruise research. In general, the increase in temperature with depth is greater in the lower half of the hole than at shallower depths.

The absolute value of the Expedition 340T downhole magnetic susceptibility correlates very well with the measured susceptibility of the core obtained during Expeditions 304 and 305. Essentially every MST peak (for smoothed data that reduces core edge artifacts) corresponds to an MSS anomaly (Fig. **F8**). Beyond the multimeter-scale correlation that we determined via shipboard analysis, more detailed documentation of the borehole thickness of oxide gabbro units will be possible. Some of the cores with this lithology had low recovery during Expeditions 304/305, as their extremely large grain size was conducive to breakup of the core into biscuit-size pieces and resulted in an unknown amount of material loss. More relevant for the goals of Expedition 340T, it appears there may be information on the relative timing of serpentinization of olivine-rich troctolite units. Using just the basic rock name from the Expedition 304/305 unit log, there is a clear association of relative lows in recorded MSS value and the olivine-rich troctolite units in the 300–350 mbsf section

(Fig. F15). This warrants further investigation, and more detailed information on both primary and alteration mineralogy should be brought to bear in analyses to determine how/whether it is serpentinization that is key or some other factor(s). If it is the serpentinized intervals that correlate with the submeter-scale drops in MSS values, then inference of an opposite polarity of the magnetic field during alteration, relative to the reversed polarity that dominated throughout cooling of the igneous section, might be appropriate.

Preliminary scientific assessment

Most components of Expedition 340T were successful, and the new data will allow us to address aspects of lithospheric hydration associated with oceanic core complex formation and evolution, as was our aim at the outset.

Two aspects of the temperature log data are relevant and are expected to help constrain new models of slow flow within narrow subsurface fault zones and broader scale (several tens to hundreds meter scale) cooling of the uplifted core of Atlantis Massif: (1) the small dips in value associated with two documented faults and (2) the distinct intervals of linear thermal gradient that differ downhole.

Sources of seismic reflectivity within the intrusive core of the massif have been identified in the Expedition 340T sonic logs. Notable impedance contrasts are associated with differences in physical properties of the olivine-rich troctolite intervals compared to surrounding lithologies. The fact that portions of these intervals are highly serpentinized means that MCS and waveform inversion methods can be expected to provide insight into the distribution of these types of subsurface hydration pathway. The combination of sonic and downhole temperature data suggests that the 750 mbsf fault zone could reflect comparable amounts of seismic energy. This will need to be assessed more carefully by modeling the volume of percolative flow needed to produce the observed temperature drop within that interval and estimating associated pore fluid volumes within the zone. Logged porosity and postcruise Stoneley wave analysis may also provide constraints in this regard.

With the data we obtained at the quietest VSP stations, an average velocity will be determined for the upper 150 m of the Central Dome, and this will allow us to address properties of the exposed detachment zone, which include hydration (alteration mineralogy) as well as deformation (porosity, in this case) that wave speeds are sensitive to.

Some of the information that we hoped to obtain as part of the zero-offset VSP experiment could not be obtained due to operational limitations.

It is likely not possible to record reflectors in this type of geologic setting with the approach used on the *JOIDES Resolution* for obtaining VSPs. The borehole seismometer needs to be decoupled from cable motion, and perhaps, environmental noise (ship? pipe against hole?) may need to be reduced in order to succeed at this next level of seismic investigation. We recommend that this information be made available to all scientists expressing interest in (at least hard rock) VSP work within IODP. Decoupling the sensor from cable motion would also reduce the likelihood of the clamping arm bending or breaking, as was experienced during two of the three VSP runs during Expedition 340T. Seas were moderate, not high, at the times of our VSP work, so our problems in this regard do not appear to reflect use in extreme conditions.

We recognize the need to comply with the designated *JOIDES Resolution* protected species mitigation plan. The PSO watches and VSP work were carried out well and in accordance with this plan. Because future IODP expeditions may benefit, we note that if we had been able to continue air gun shots into the evening hours on 24 February, our VSI data set may have been significantly better than it is. For whatever combination of reasons (clamping arm not bent? less ship/cable noise?) the 24 February VSP run was the only one to produce consistently good quality data. Acquisition might have extended to additional (and deeper) stations if we had been able to continue under those conditions. For projects where VSP work is of high priority, IODP may want to explore developing a mitigation plan designed to allow evening seismic source operations.

Less-than-optimum selection of design, possibly material, of the centralizer arms impacted our operations. If we had not arrived on site early, due to very rapid transit, and if the USIO had not been willing to allow us to use this extra time for our work, we would have failed in our attempt to document the seismic properties of the lower portion of Hole U1309D. About 2 days were required for our team to recognize and learn how to address this problem in order to have successful DSI and VSI runs.

Higher than usual (for IODP) temperature in this hole may be a factor in the significant wear and failure of the centralizer arms. It is not out of the question that borehole chemistry also played a role (but this has not been tested), since Lost City hydrothermal vent field a few kilometers south of Site U1309 is known to have high-

pH fluid. Measured fluid resistivity in the borehole does deviate from standard seawater values in the lower parts of the hole.

The rapid transit from Lisbon, Portugal, to Site U1309 introduced an unexpected set of activities—the potential for extra time on site meant that additional science related to both Expeditions 340T and 304/305 might be addressed. The ship's management, technical and drill crews, and onshore personnel were all very helpful as we explored this possibility. Their willingness to adjust onboard workflow during Expedition 340T to accommodate a modest amount of unexpected coring is recognized and very much appreciated. In the end just a single sampling effort was possible; even this reflected the onboard group's ability to be creative in order to take advantage of a scientific opportunity. By rigging a modified APC bit/barrel and deploying it from 150 m above seafloor within the drill pipe, we obtained what was essentially a gravity core. The fragments of rock and gravel recovered show promise for providing worthwhile geochemical and microstructural information on the uppermost surface of the detachment exposed on the dome of Atlantis Massif.

References

Arnulf, A., 2011. Layer 2A structure beneath the Lucky Strike Volcano, Mid-Atlantic Ridge, from high-resolution tomography and full waveform inversion [Ph.D. thesis]. Institut de Physique du Globe de Paris.

Bartetzko, A., Paulick, H., Iturrino, G., and Arnold, J., 2003. Facies reconstruction of a hydrothermally altered dacite extrusive sequence: evidence from geophysical downhole logging data (ODP Leg 193). *Geochem., Geophys., Geosyst.,* 4(10):1087. **doi:10.1029/2003GC000575**

Beard, J.S., Frost, B.R., Fryer, P., McCaig, A., Searle, R., Ildefonse, B., Zinin, P., and Sharma, S.K., 2009. Onset and progression of serpentinization and magnetite formation in olivine-rich troctolite from IODP Hole U1309D. *J. Petrol.,* 50(3):387–403. **doi:10.1093/petrology/egp004**

Blackman, D.K., Canales, J.P., and Harding, A., 2009. Geophysical signatures of oceanic core complexes. *Geophys. J. Int.,* 178(2):593–613. **doi:10.1111/j.1365-246X.2009.04184.x**

Blackman, D.K., Ildefonse, B., John, B.E., Ohara, Y., Miller, D.J., Abe, N., Abratis, M., Andal, E.S., Andreani, M., Awaji, S., Beard, J.S., Brunelli, D., Charney, A.B., Christie, D.M., Collins, J., Delacour, A.G., Delius, H., Drouin, M., Einaudi, F., Escartín, J., Frost, B.R., Früh-Green, G., Fryer, P.B., Gee, J.S., Godard, M., Grimes, C.B., Halfpenny, A., Hansen, H.-E., Harris, A.C., Hayman, N.W., Hellebrand, E., Hirose, T., Hirth, J.G., Ishimaru, S., Johnson, K.T.M., Karner, G.D., Linek, M., MacLeod, C.J., Maeda, J., Mason, O.U., McCaig, A.M., Michibayashi, K., Morris, A., Nakagawa, T., Nozaka, T., Rosner, M., Searle, R.C., Suhr, G., Tominaga, M., von der Handt, A., Yamasaki, T., and Zhao, X., 2011. Drilling constraints on lithospheric accretion and evolution at Atlantis Massif, Mid-Atlantic Ridge 30°N. *J Geophys. Res., [Solid Earth],* 116:B07103. **doi:10.1029/2010JB007931**

Blackman, D.K., Ildefonse, B., John, B.E., Ohara, Y., Miller, D.J., MacLeod, C.J., and the Expedition 304/305 Scientists, 2006. *Proc IODP,* 304/305: College Station, TX (Integrated Ocean Drilling Program Management International, Inc.). **doi:10.2204/iodp.proc.304305.2006**

Blackman, D.K., Karner, G.D., and Searle, R.C., 2008. Three-dimensional structure of oceanic core complexes: effects on gravity signature and ridge flank morphology, Mid-Atlantic Ridge, 30°N. *Geochem., Geophys., Geosyst.,* 9(6):Q06007. **doi:10.1029/2008GC001951**

Blackman, D.K., Karson, J.A., Kelley, D.S., Cann, J.R., Früh-Green, G.L., Gee, J.S., Hurst, S.D., John, B.E. Morgan, J., Nooner, S.L., Ross, D.K., Schroeder, T.J., and Williams, E.A., 2002. Geology of the Atlantis Massif (Mid-Atlantic Ridge, 30°N): implications for the evolution of an ultramafic oceanic core complex. *Mar. Geophys. Res.,* 23(5–6):443–469. **doi:10.1023/B:MARI.0000018232.14085.75**

Bonatti, E., and Honnorez, J., 1976. Sections of the Earth's crust in the equatorial Atlantic. *J. Geophys. Res., [Solid Earth],* 81(23):4104–4116. **doi:10.1029/JB081i023p04104**

Boschi, C., Früh-Green, G.L., Delacour, A., Karson, J.A., and Kelley, D.S., 2006. Mass transfer and fluid flow during detachment faulting and development of an oceanic core complex, Atlantis Massif (MAR 30°N). *Geochem., Geophys., Geosyst.,* 7(1):Q01004. **doi:10.1029/2005GC001074**

Canales, J.P., Tucholke, B.E., and Collins, J.A., 2004. Seismic reflection imaging of an oceanic detachment fault: Atlantis megamullion (Mid-Atlantic Ridge, 30°10′N). *Earth Planet. Sci. Lett.,* 222(2):543–560. **doi:10.1016/j.epsl.2004.02.023**

Canales, J.P., Tucholke, B.E., Xu, M., Collins, J.A., and DuBois, D.L., 2008. Seismic evidence for large-scale compositional heterogeneity of oceanic core complexes. *Geochem., Geophys., Geosyst.,* 9:Q08002. **doi:10.1029/2008GC002009**

Cann, J.R., Blackman, D.K., Smith, D.K., McAllister, E., Janssen, B., Mello, S., Avgerinos, E., Pascoe, A.R., and Escartin, J., 1997. Corrugated slip surfaces formed at ridge–transform intersections on the Mid-Atlantic Ridge. *Nature (London, U. K.),* 385(6614):329–332. **doi:10.1038/385329a0**

Cannat, M., 1993. Emplacement of mantle rocks in the seafloor at mid-ocean ridges. *J. Geophys. Res., [Solid Earth],* 98(B3):4163–4172. **doi:10.1029/92JB02221**

Collins, J.A., Blackman, D.K., Harris, A., and Carlson, R.L., 2009. Seismic and drilling constraints on velocity structure and reflectivity near IODP Hole U1309D on the Central Dome of Atlantis Massif, Mid-Atlantic Ridge 30°N. *Geochem., Geophys., Geosyst.,* 10:Q01010. **doi:10.1029/2008GC002121**

Dick, H.J.B., 1989. Abyssal peridotites, very slow spreading ridges and ocean ridge magmatism. *In* Saunders, A.D., and Norry, M.J. (Eds.), *Magmatism in the Ocean Basins*. Geol. Soc. Spec. Publ., 42(1):71–105. **doi:10.1144/GSL.SP.1989.042.01.06**

Ellis, D.V., and Singer, J.M., 2007. *Well Logging for Earth Scientists,* (2nd ed.): New York (Elsevier).

Früh-Green, G.L., Kelley, D.S., Bernasconi, S.M., Karson, J.A., Ludwig, K.A., Butterfield, D.A., Boschi, C., and Proskurowksi, G., 2003. 30,000 years of hydrothermal activity at the Lost City vent field. *Science,* 301(5632):495–498. **doi:10.1126/science.1085582**

Goldberg, D., 1997. The role of downhole measurements in marine geology and geophysics. *Rev. Geophys.,* 35(3):315–342. **doi:10.1029/97RG00221**

Grimes, C.B., John, B.E., Cheadle, M.J., and Wooden, J.L., 2008. Protracted construction of gabbroic crust at a slow spreading ridge: constraints from $^{206}Pb/^{238}U$ zircon ages from Atlantis Massif and IODP Hole U1309D (30°N, MAR). *Geochem., Geophys., Geosyst.,* 9:Q08012. **doi:10.1029/2008GC002063**

Henig, A.S., Blackman, D.K., Harding, A.J., Canales, J.-P., and Kent, G.M., in press. Downward continued multichannel seismic refraction analysis of Atlantis Massif oceanic core complex, 30°N Mid-Atlantic Ridge. *Geochem., Geophys., Geosyst.*

Henig, A.S., Blackman, D.K., Harding, A.J., and Kent, G., 2010. Seismic structure and inferred lithology of the heterogeneous upper lithosphere at Atlantis Massif Oceanic Core Complex, 30°N MAR [presented at the American Geophysical Union Fall 2010 Meeting, San Francisco, CA, 13–17 December 2010]. (Abstract T23A-2225) **http://www.agu.org/meetings/fm10/waisfm10.html**

Hirose, T., and Hayman, N.W., 2008. Structure, permeability, and strength of a fault zone in the footwall of an oceanic core complex, the Central Dome of the Atlantis Massif, Mid-Atlantic Ridge, 30°N. *J. Struct. Geol.,* 30(8):1060–1071. **doi:10.1016/j.jsg.2008.04.009**

Hornby, B.E., Johnson, D.L., Winkler, K.W., and Plumb, R.A., 1989. Fracture evaluation using reflected Stoneley-wave arrivals. *Geophysics,* 54(10):1274–1288. **doi:10.1190/1.1442587**

Ildefonse, B., Blackman, D.K., John, B.E., Ohara, Y., Miller, D.J., MacLeod, C.J., and Integrated Ocean Drilling Program Expeditions 304/305 Science Party, 2007. Oceanic core complexes and crustal accretion at slow-spreading ridges. *Geology,* 35(7):623–626. **doi:10.1130/G23531A.1**

John, B.E., 1987. Geometry and evolution of a mid-crustal extensional fault system: Chemehuevi Mountains, southeastern California. *In* Coward, M.P., Dewey, J.F., and Hancock P.L.

(Eds.), *Continental Extensional Tectonics*. Geol. Soc. Spec. Publ., 28:313–335. **doi:10.1144/GSL.SP.1987.028.01.20**

Jones, G.D., Barton, P.J., and Singh, S.C., 2007. Velocity images from stacking depth-slowness seismic wavefields. *Geophys. J. Int.,* 168(2):583–592. **doi:10.1111/j.1365-246X.2006.03055.x**

Karson, J.A., Früh-Green, G.L., Kelley, D.S., Williams, E.A., Yoerger, D.R., and Jakuba, M., 2006. Detachment shear zone of the Atlantis Massif core complex, Mid-Atlantic Ridge, 30°N. *Geochem., Geophys., Geosyst.,* 7(6):Q06016. **doi:10.1029/2005GC001109**

Kelley, D.S., Karson, J.A., Blackman, D.K., Früh-Green, G.L., Butterfield, D.A., Lilley, M.D., Olson, E.J., Schrenk, M.O., Roe, K.K., Lebon, G.T., Rivizzigno, P., and the AT3-60 Shipboard Party, 2001. An off-axis hydrothermal vent field near the Mid-Atlantic Ridge at 30°N. *Nature (London, U. K.),* 412(6843):145–149. **doi:10.1038/35084000**

Kimball, C.V., and Marzetta, T.L., 1984. Semblance processing of borehole acoustic array data. *Geophysics,* 49(3):274–281. **doi:10.1190/1.1441659**

Lagabrielle, Y., Bideau, D., Cannat, M., Karson, J.A., and Mével, C., 1998. Ultramafic-mafic plutonic rock suites exposed along the Mid-Atlantic Ridge (10°N–30°N): symmetrical-asymmetrical distribution and implications for seafloor spreading processes. *In* Buck, W.R., Delaney, P.T., Karson, J.A., and Labagrielle, Y. (Eds.), *Faulting and Magmatism and Mid-Ocean Ridges*. Geophys. Monogr., 106:153–176. **doi:10.1029/GM106p0153**

Lin, J., Purdy, G.M., Schouten, H., Sempéré, J.-C., and Zervas, C., 1990. Evidence from gravity data for focused magmatic accretion along the Mid-Atlantic Ridge. *Nature (London, U. K.),* 344(6267):627–632. **doi:10.1038/344627a0**

Lovell, M.A., Harvey, P.K., Brewer, T.S., Williams, C., Jackson, P.D., and Williamson, G., 1998. Application of FMS images in the Ocean Drilling Program: an overview. *In* Cramp, A., MacLeod, C.J., Lee, S.V., and Jones, E.J.W. (Eds.), *Geological Evolution of Ocean Basins: Results from the Ocean Drilling Program*. Geol. Soc. Spec. Publ., 131(1):287–303. **doi:10.1144/GSL.SP.1998.131.01.18**

Masoomzadeh, H., Barton, P.J., and Singh, S.C., 2005. Advanced processing of long-offset seismic data for sub-basalt imaging in the Faeroe-Shetland Basin. *SEG Expanded Abstr.,* 25:417–420. **doi:10.1190/1.2142230**

McCaig, A.M., Delacour, A., Fallick, A.E., Castelain, T., and Früh-Green, G.L., 2010. Detachment fault control on hydrothermal circulation systems: interpreting the subsurface beneath the TAG hydrothermal field using the isotopic and geological evolution of oceanic core complexes in the Atlantic. *In* Rona, P.A., Devey, C.W., Dyment, J., and Murton, B.J. (Eds.), *Diversity of Hydrothermal Systems on Slow Spreading Ocean Ridges*. Geophys. Monogr., 188:207–239. **doi:10.1029/2008GM000729**

Michibayashi, K., Hirose, T., Nozaka, T., Harigane, Y., Escartin, J., Delius, H., Linek, M., and Ohara, Y., 2008. Hydration due to high-T brittle shear within in situ oceanic crust, 30°N Mid-Atlantic Ridge. *Earth Planet. Sci. Lett.,* 275(3–4):348–354. **doi:10.1016/j.epsl.2008.08.033**

OTTER (Oceanographer Tectonic Research Team), Karson, J.A., Fox, P.J., Sloan, H., Crane, K.T., Kidd, W.S.F., Bonatti, E., Stroup, J.B., Fornari, D.J., Elthon, D., Hamlyn, P., Casey, J.F., Gallo, D.G., Needham, D., and Sartori, R., 1984. The geology of the Oceanographer Transform: the ridge-transform intersection. *Mar. Geophys. Res.,* 6(2):109–141. **doi:10.1007/BF00285956**

Rider, M.H., 1996. *The Geological Interpretation of Well Logs* (2nd ed.): Caithness (Whittles Publ.).

Schlumberger, 1989. *Log Interpretation Principles/Applications:* Houston (Schlumberger Educ. Serv.), SMP–7017.

Schroeder, T., and John, B.E., 2004. Strain localization on an oceanic detachment fault system, Atlantis Massif, 30°N, Mid-Atlantic Ridge. *Geochem., Geophys., Geosyst.,* 5:Q11007. **doi:10.1029/2004GC000728**

Serra, O., 1984. *Fundamentals of Well-Log Interpretation* (Vol. 1): *The Acquisition of Logging Data:* Amsterdam (Elsevier).

Serra, O., 1986. *Fundamentals of Well-Log Interpretation* (Vol. 2): *The Interpretation of Logging Data*. Amsterdam (Elsevier).

Serra, O., 1989. *Formation MicroScanner Image Interpretation:* Houston (Schlumberger Educ. Serv.), SMP-7028.

Singh, S.C., Collins, J.A., Canales, J.P., Tucholke, B.E., and Detrick, R.S., 2004. New insights into serpentinization at Atlantis Massif, 30°N Mid-Atlantic Ridge, using wide-angle seismic method. *Eos, Trans. Am. Geophys. Union,* 85(47)(Suppl.):V23B-0628. (Abstract) **http://www.agu.org/meetings/fm04/waisfm04.html**

Sinton, J.M., and Detrick, R.S., 1992. Mid-ocean ridge magma chambers. *J. Geophys. Res., [Solid Earth],* 97(B1):197–216. **doi:10.1029/91JB02508**

Tucholke, B.E., Lin, J., and Kleinrock, M.C., 1998. Megamullions and mullion structure defining oceanic metamorphic core complexes on the Mid-Atlantic Ridge. *J. Geophys. Res., [Solid Earth],* 103(B5):9857–9866. **doi:10.1029/98JB00167**

White, R.S., McKenzie, D., and O'Nions, R.K., 1992. Oceanic crustal thickness from seismic measurements and rare earth element inversions. *J. Geophys. Res., [Solid Earth],* 97(B13):19683–19715. **doi:10.1029/92JB01749**

Table T1. Downhole measurements made by the wireline tool strings during IODP Expedition 340T.

Tool string	Tool	Measurement	Sampling interval (cm)	Vertical resolution (cm)
Triple combo	LEH-MT	Temperature	15	NA
	EDTC	Total gamma ray	5 and 15	30
	HLDS	Bulk density	2.5 and 15	38
	HRLA	Resistivity	15	30
	MTT	Temperature	15	NA
Sonic	LEH-MT	Temperature	15	NA
	EDTC	Total gamma ray	5 and 15	30
	DSI	Acoustic velocity	15	107
	GPIT	Tool orientation and acceleration	4	15
Magnetic susceptibility	LEH-MT	Temperature	15	NA
	EDTC	Total gamma ray	5 and 15	30
	MSS	Magnetic susceptibility	2.54	40
Versatile Seismic Imager	LEH-MT	Temperature	15	NA
	VSI	One-way acoustic traveltime	Stations at 10–20 m	NA
	EDTC	Total gamma ray	5 and 15	30

All tool and tool string names except the MTT and MSS are trademarks of Schlumberger. Sampling interval based on optimal logging speed. Acoustic imaging approximate vertical resolution is at 500 kHz. NA = not applicable. For definitions of tool acronyms, see Table **T3.**

Table T2. Chronology of logging operations in Hole U1309D during Expedition 340T. (Continued on next page.)

Operation	Date (Feb 2012)	Time (ship local)	Depth (mbrf)	Comments
Run 1: triple combo tool string				
Rig floor preparation	21	1440		
Tool string rig up	21	1510		
Tool string check	21	1535		Computer swapped after failure to start HLDS because of EDTC patch
Tool string RIH	21	1620	0	Started 1500 ft/h; sped up to 6000 ft/h below 100 mbrf
Pause at seafloor	21	1730	1700	Purpose was to stabilize tool temperature to limit influence on temperature log
Tool string at EOP	21	1800	1711	Start downlog
Turn on WHC	21	1805	1755	
Turn off WHC	21	1825	1900	WHC motion choppy; not much heave to compensate, so not necessary
End downlog	21	2103	3060	Maximum temperature at bottom = 144.6°C (MTT)
Begin uplog Pass 1	21	2105	3060	Tight hole (~5 inches) with first caliper readings
End uplog Pass 1	21	2130	2900	Tool sent back to TD 3000 ft/h
Begin uplog Pass 2	21	2140	3048	Could not go deeper than 3048 mbrf; likely tight hole
Close caliper	22	035	1750	Go back down to 1800 mbrf to fix spooling
Pull into pipe	22	045	1737	
Tool string inside pipe	22	050	1711	Tool mostly inside pipe; impossible to pull further
End of Pass 2	22	516	1711	
Kinley operations				
Kinley crimper RIH	22	655		Based on depth, it takes an hour to work tool down
Kinley hammer RIH	22	800		
Kinley crimper 2 RIH	22	900		Tool did not lose power after first crimper; may have not worked
Kinley hammer RIH	22	1000		
Kinley cutter RIH	22	1035		
Kinley hammer RIH	22	1145		Wireline severed at 1200 h; pulled to surface
End of wireline on deck	22	1330		Start tripping pipe; camera run to seafloor to check position of tools
Tool string at surface	22	1715	0	MTT and bottom of HRLA sticking out of bit
Rig floor clear	22	1930		
Run 2: VSI				
Start protected species watch	23	600		
Rig floor preparation	23	800		
Tool string rig up	23	815		
Tool string RIH	23	835	0	Started at 1500 ft/h; sped up to 4000 ft/h below ~100 mbrf
Tool string at EOP	23	1010		Apparent ledge at ~1718 mbrf; passed at 1025 h; other tight spot 1746 mbrf
Stop to calibrate GR depth	23	1040	1916.0	Stop at 1916 mbrf to log up across a peak in GR to match depths with triple combo
First station	23	1100	1804.6	First shot fired at 1105 h; following shots to tune (sync) the two guns
Continue descent	23	1118	1804.6	First station complete
Turn on WHC	23	1128		WHC turned on to check efficiency and evaluate noise on geophone
Test WHC	23			WHC not helping; turned off at 1138 h
Reach TD	23	1225	3040	
Begin uplog Pass 1	23	1235	3016–2966	Stations tried at 3016, 3014, 3004, 2990, and 2966 mbrf; no success
Pull up	23	1335		Decide to try at shallower depth
Last station	23	1355	2716	Attempt to renew success of first station; no luck; assume tool damaged
Pull up	23	1358	2716	
Pull tool string into pipe	23	1435	1708	Trouble at bit confirms damaged arm; pulled 3000 lb (head tension) to come through
Check tool opening	23	1445	1655	Try to open arm; indicates >17 inches; arm definitely damaged
Tool string at surface	23	1535	0	VSI is missing extension arm; shuttles swapped for following run in the remaining daylight
Run 3: VSI				
Tool string rig up	23	1600		
Tool string RIH	23	1605	0	
Stop to calibrate GR depth	23	1700	1840	Stop to match depth with main triple combo pass across GR peak; shifted 3 m
First station	23	1705	1782	Noisy signal; three successful station recorded between 1782 and 1742 mbrf
Pull into pipe	23	1735	1711	No problem
Station in pipe	23	1740	1696	Noisy; more attempts at 1656 mbrf; last shot fired at 1759 h
Pull tool to surface	23	1800	1656	
Tool string at surface	23	1853	0	Arm slightly bent - will be straightened overnight
Tools rigged down	23	1905		
Rig floor clear	23	1910		Rig floor cleared for tripping pipe down to 2356 mbrf (700 mbsf) for sonic
Run 4: sonic				
Rig floor preparation	23	2200		
Tool string rig up	23	2215		
Tool string check	23	2230		
Tool string RIH	23	2245	0	Pick up speed to 6000 ft/h below 100 mbrf; stop to test tension at 2325 mbrf
Start downlog	24	014	2323	Losing head tension at 2345 mbrf (11 m above bit); could not go deeper
End downlog	24	113	2345	Apply ~2000 lb overpull to move tools, continue overpull through BHA
Run up in pipe	24	117	2298	Normal head tension return once out of BHA in normal diameter pipe
Tool string at surface	24	255		Inspect string - centralizers intact (no noticeable wear from pipe)

Table T2 (continued).

Operation	Date (Feb 2012)	Time (ship local)	Depth (mbrf)	Comments
Tools rigged down	24	330		
Rig floor cleared	24	335		Rig floor cleared for tripping pipe up to 1759 mbrf (below tight spots) for VSI
Run 5: VSI				
Rig floor preparation	24	600		Prepare rig floor after deployment of XCB core barrel to confirm that pipe is clear
Start protected species watch	24	630		
Tool string rig up	24	705		
Tool string check	24	720		
Tool string RIH	24	725	0	Started at 2000 ft/h down to ~100 mbrf, then sped up
Tool string at EOP	24	827	1759	
GR matching pass	24	832	1850	Stop to log up, shift depth to match GR from previous run (2.8 m shift)
Continue downlog pass	24	844	1820	
Turn on WHC	24	849	1820	Modify some WHC parameters, trying to smooth jerky up-motion
RIH to TD	24	910		Ledge at 2412 m, worked past it
Reach TD	24	950	3020	Chose a point below deepest station to stop, then run up
Begin VSP stations	24	952	3016	First, deepest station at 3016 mbrf and continue up
Turn off WHC	24	1305	2596	Test WHC by turning off for three stations, shots are still noisy
Turn on WHC	24	1335	2513	Turn WHC on again because it is not making things worse
Final VSP station	24	1701	1832	Last shots fired at 1705 h
Turn off WHC	24	1712		Turn off WHC and run up to pipe depth; caliper only closing to 9 inches
Pull into pipe	24	1720	1759	Some head tension entering pipe/passing through BHA; caliper is bent but closes to 3 inches
Everything past bit and Kinley sub	24	1729	1725	End of pass
Run up	24	1730	1725	Head tension back to normal; slow to 4000 ft/h at 200 mbrf, to 2000 ft/h at 70 mbrf
Tool string at surface	24	1836	0	Confirm that caliper is slightly bent
Tools rigged down	24	1845		Rig floor cleared for tripping pipe down to 2356 mbrf for second sonic log attempt
Run 6: sonic				
Tool string rig up	24	2020		
Tool string check	24	2040		
Tool string RIH	24	2045	0	Pick up speed to 7000 ft/h below 50 mbrf
Start downlog	24	2217	2333	Slow to 1100 ft/h just above bit
Tool string at EOP	24	2225	2380	No trouble through BHA or bit
Turn on WHC	24	2230	2400	Turn on WHC
Reach TD; end downlog	25	027	3040	Ledge at 3040 mbrf; can't pass so this is TD
Begin uplog Pass 1	25	031	3040	
Turn off WHC	25	226	2392	
Pull into pipe	25	236	2365	
End uplog Pass 1	25	241	2321	
Run up in pipe	25	245	2321	No problems with Kinley sub or BHA; run up in pipe at 6000 ft/h
Tool string at surface	25	405	0	
Tools rigged down	25	430		
Rig floor cleared	25	435		Rig floor cleared for tripping pipe back up to 1759 mbrf for final MSS run
Run 7: MSS				
Tool string rig up	25	600		
Tool string check	25	605		
Tool string RIH	25	615	0	
Start downlog	25	655	1732	
Tool string at EOP	25	700	1759	
Turn on WHC	25	705	1815	Turn on WHC and continue RIH at 5000 ft/h
Reach TD; end downlog	25	729	2419	Depth of thermal limit for tool (80°C), LEH-MT = 75°C
Begin uplog Pass 1	25	731	2419	Fast main pass
End uplog Pass 1	25	757	1761	Complete main pass; RIH to 500 mbsf for repeat pass
Begin uplog Pass 2	25	809	2165	Slow repeat pass at 1500 ft/h
Turn off WHC	25	901	1795	
Pull into pipe	25	902	1759	No problems coming into bit, or with Kinley sub or BHA
Reach seafloor (up)	25	910	1637	
End uplog Pass 2	25	910	1637	Run up in pipe at 5000 ft/h
Tool string at surface	25	1000	0	End calibration for EDTC-B ~10 min
Tools rigged down	25	1015		
Rig floor cleared	25	1022		

Ship local time = UTC – 2. RIH = run in hole, EOP = end of pipe, WHC = wireline heave compensator, HLDS = Hostile Environment Litho-Density Sonde, EDTC = Enhanced Digital Telemetry Cartridge, MTT = Modular Temperature Tool, VSI = Versatile Seismic Imager, HLRA = High-Resolution Laterolog Array, MSS = Magnetic Susceptibility Sonde, TD = total depth, GR = gamma ray, BHA = bottom-hole assembly, XCB = extended core barrel, LEH-MT = logging equipment head–mud temperature.

Table T3. Acronyms and units used for downhole wireline tools and measurements.

Tool	Output	Description	Unit
LEH-MT		Logging equipment head with tension and mud temperature	
	MTEM	Borehole fluid temperature	°C
	TENS	Cablehead tension	lb
EDTC		Enhanced Digital Telemetry Cartridge	
	GR	Total gamma ray	gAPI
	ECGR	Environmentally corrected gamma ray	gAPI
	EHGR	High-resolution environmentally corrected gamma ray	gAPI
	MTEM	Borehole fluid temperature	°C
HLDS		Hostile Environment Litho-Density Sonde	
	RHOM	Bulk density	g/cm^3
	PEFL	Photoelectric effect	$barn/e^-$
	LCAL	Caliper (measure of borehole diameter)	Inch
	DRH	Bulk density correction	g/cm^3
HRLA		High-Resolution Laterolog Array	
	RLAXXX	Apparent resistivity from computed focusing Mode XXX	Ωm
	RT	True resistivity	Ωm
	MRES	Borehole fluid resistivity	Ωm
MTT		Modular Temperature Tool	
	WTEP	Borehole fluid temperature	°C
GPIT		General Purpose Inclinometry Tool	
	DEVI	Hole deviation	Degrees
	HAZI	Hole azimuth	Degrees
	Fx, Fy, Fz	Earth's magnetic field (three orthogonal components)	Degrees
	Ax, Ay, Az	Acceleration (three orthogonal components)	m/s^2
DSI		Dipole Sonic Imager	
	DTCO	Compressional wave slowness	µs/ft
	DTSM	Shear wave slowness	µs/ft
	DT1	Shear wave slowness, lower dipole	µs/ft
	DT2	Shear wave slowness, upper dipole	µs/ft
VSI		Versatile Seismic Imager	
	1WTT	Acoustic traveltime	s
MSS		Magnetic susceptibility	
	LSUS	Magnetic susceptibility, deep reading	Uncalibrated units

Table T4. Quality of Expedition 340T VSP traces for each seismometer component. (Continued on next two pages.)

VSP station	Depth (mbsf)	Shot number	Time* Julian day (2012)	Time* (hh:mm:ss)	Quality *x*	Quality *y*	Quality *z*
3	86	76	53	15:21:32	3	3	2
3	86	80	53	15:22:50	3	3	3
3	86	81	53	15:23:08	0	0	1
3	86	82	53	15:23:26	4	4	4
3	86	83	53	15:23:44	4	4	4
3	86	84	53	15:24:06	3	3	3
3	86	85	53	15:24:25	1	1	1
3	86	88	53	15:25:57	2	1	3
3	86	93	53	15:27:55	3	3	4
3	86	96	53	15:28:49	2	3	3
3	86	97	53	15:29:07	3	2	3
4	100	66	53	15:14:04	4	3	3
4	100	68	53	15:14:40	4	4	4
4	100	69	53	15:14:58	4	4	4
4	100	70	53	15:15:16	1	2	2
4	100	71	53	15:15:34	4	3	3
4	100	72	53	15:15:52	3	3	4
5	126	55	53	15:07:08	0	0	1
5	126	57	53	15:07:45	3	3	4
5	126	60	53	15:08:40	3	4	4
5	126	62	53	15:09:16	2	2	4
5	126	63	53	15:09:34	2	2	4
5	126	64	53	15:09:52	0	0	2
6	150	3	53	09:04:45	3	2	4
6	150	4	53	09:05:15	4	3	4
6	150	5	53	09:06:17	1	0	1
6	150	6	53	09:06:48	1	1	2
6	150	7	53	09:08:05	2	0	3
6	150	8	53	09:08:23	4	4	4
6	150	9	53	09:08:42	0	0	1
6	150	10	53	09:09:15	3	3	4
6	150	11	53	09:09:33	4	4	4
6	150	12	53	09:09:51	4	4	4
6	150	13	53	09:10:21	3	2	4
6	150	14	53	09:10:39	4	4	4
6	150	15	53	09:11:06	4	3	4
6	150	16	53	09:13:05	4	3	4
6	150	17	53	09:13:56	3	2	3
6	150	18	53	09:14:26	3	2	3
6	150	20	53	09:15:05	4	4	4
6	150	22	53	09:15:42	3	2	4
8	210	662	54	14:57:29	0	0	1
8	210	663	54	14:57:47	1	1	1
9	236	652	54	14:51:01	0	1	1
9	236	653	54	14:51:19	1	1	0
9	236	655	54	14:51:55	1	1	0
9	236	656	54	14:52:13	1	1	1
10	266	641	54	14:43:29	2	0	1
10	266	642	54	14:43:47	1	1	1
10	266	643	54	14:44:05	1	1	0
10	266	646	54	14:45:00	1	1	1
10	266	648	54	14:45:36	1	0	1
10	266	649	54	14:45:54	1	1	1
11	292	632	54	14:36:56	0	0	1
11	292	633	54	14:37:15	1	1	1
12	315	621	54	14:28:24	3	2	0
12	315	623	54	14:29:00	1	1	1
12	315	626	54	14:29:54	1	1	0
12	315	628	54	14:30:30	1	1	1
13	345	612	54	14:20:35	2	2	0
13	345	614	54	14:21:12	1	1	1
13	345	615	54	14:21:30	0	1	3
13	345	617	54	14:22:06	0	0	1
13	345	618	54	14:22:24	0	0	3
14	356	601	54	14:12:18	0	0	1
14	356	602	54	14:12:36	1	0	0
14	356	604	54	14:13:12	3	3	3

Table T4 (continued). (Continued on next page.)

VSP station	Depth (mbsf)	Shot number	Time* Julian day (2012)	Time* (hh:mm:ss)	Quality *x*	Quality *y*	Quality *z*
14	356	609	54	14:14:42	3	3	3
15	382	593	54	14:05:57	0	0	3
15	382	595	54	14:06:33	3	3	3
15	382	597	54	14:07:09	1	2	3
15	382	598	54	14:07:27	0	1	4
15	382	600	54	14:08:03	2	2	0
16	399	582	54	13:57:57	1	1	0
16	399	586	54	13:59:26	3	2	4
16	399	589	54	14:00:20	1	0	1
17	422	571	54	13:49:47	0	1	1
17	422	575	54	13:50:59	0	0	1
17	422	577	54	13:51:35	1	1	0
18	444	561	54	13:40:13	1	1	0
18	444	565	54	13:41:27	3	3	3
18	444	568	54	13:42:21	0	0	1
19	472	551	54	13:33:06	1	1	1
19	472	552	54	13:33:34	0	0	2
19	472	553	54	13:33:52	3	2	4
19	472	554	54	13:34:10	3	3	2
19	472	555	54	13:34:28	0	0	3
19	472	560	54	13:35:59	2	2	2
20	500	542	54	13:24:03	0	1	1
20	500	543	54	13:24:24	0	0	2
21	530	536	54	13:17:08	3	3	4
21	530	537	54	13:17:51	1	1	0
21	530	539	54	13:18:34	1	0	0
22	554	525	54	13:08:06	1	1	3
23	577	514	54	13:00:23	3	3	4
23	577	516	54	13:01:20	0	0	3
23	577	518	54	13:01:56	3	3	4
23	577	520	54	13:02:35	0	0	3
24	597	502	54	12:48:12	3	3	4
24	597	504	54	12:48:48	3	2	4
24	597	506	54	12:49:31	3	3	4
25	624	493	54	12:40:27	2	2	2
26	649	481	54	12:32:08	3	2	4
26	649	489	54	12:35:43	1	1	2
26	649	490	54	12:36:01	4	4	4
27	677	474	54	12:25:32	0	0	3
27	677	475	54	12:26:05	2	2	2
27	677	477	54	12:26:41	3	3	3
29	735	452	54	12:10:09	0	0	3
29	735	458	54	12:11:58	1	1	3
29	735	459	54	12:12:16	2	2	3
29	735	460	54	12:12:34	0	0	3
30	760	446	54	12:02:24	3	3	4
30	760	448	54	12:03:01	2	2	3
30	760	450	54	12:03:37	1	1	0
31	788	431	54	11:52:20	1	1	1
31	788	434	54	11:53:16	1	0	3
31	788	435	54	11:53:35	0	0	1
31	788	438	54	11:54:29	2	2	2
32	816	425	54	11:46:55	1	0	2
32	816	427	54	11:47:31	1	1	3
32	816	429	54	11:48:08	1	1	0
32	816	430	54	11:48:28	1	1	4
33	835	411	54	11:39:10	3	3	4
33	835	412	54	11:39:28	2	3	4
33	835	414	54	11:40:04	0	0	2
33	835	417	54	11:41:02	3	3	4
33	835	418	54	11:41:20	0	2	4
33	835	419	54	11:41:38	1	1	0
34	857	403	54	11:32:51	0	0	2
35	884	392	54	11:18:35	0	1	0
35	884	397	54	11:20:05	0	0	3
35	884	400	54	11:21:00	0	1	3
36	912	380	54	11:08:56	1	1	0
36	912	381	54	11:09:14	2	2	2

Table T4 (continued).

VSP station	Depth (mbsf)	Shot number	Time* Julian day (2012)	Time* (hh:mm:ss)	Quality *x*	Quality *y*	Quality *z*
36	912	383	54	11:09:50	0	0	3
36	912	385	54	11:10:32	3	4	4
37	940	365	54	10:58:37	0	0	3
37	940	367	54	10:59:13	0	0	1
37	940	374	54	11:01:21	3	3	4
38	965	356	54	10:50:54	0	0	3
38	965	359	54	10:52:01	1	1	1
39	990	337	54	10:41:24	1	1	0
39	990	344	54	10:43:32	1	1	0
40 1	29	322	54	10:31:51	0	1	3
40 1	29	329	54	10:33:58	0	0	1
41 1	60	311	54	10:23:28	0	0	1
42 1	90	307	54	10:18:31	1	1	1
43 1	120	285	54	10:01:53	2	1	2
43 1	120	288	54	10:02:51	1	0	0
44 1	146	278	54	09:53:04	1	0	0
45 1	170	258	54	09:37:43	0	0	4
45 1	170	259	54	09:38:01	0	0	3
45 1	170	261	54	09:38:37	1	1	1
45 1	170	264	54	09:39:32	1	0	3
45 1	170	268	54	09:40:44	0	0	3
47 1	216	224	54	09:18:46	0	0	3
47 1	216	227	54	09:20:01	2	1	4
47 1	216	229	54	09:20:37	1	1	1
47 1	216	231	54	09:21:14	2	2	3
49 1	260	197	54	08:59:55	3	3	4
49 1	260	205	54	09:02:44	3	2	4
50 1	285	185	54	08:50:33	0	1	3
50 1	285	188	54	08:51:27	0	0	1
50 1	285	189	54	08:51:45	1	1	1
51 1	310	168	54	08:39:55	0	0	1
51 1	310	170	54	08:40:32	1	1	1
51 1	310	173	54	08:41:30	0	0	1
52 1	334	151	54	08:28:27	1	1	1
52 1	334	158	54	08:31:12	0	0	3
55 1	360	137	54	08:17:51	0	0	3
55 1	360	138	54	08:18:09	0	0	1
55 1	360	140	54	08:19:17	0	0	1

* = listed in SEGY header, which is UTC – 5. Quality ranking is 0–4, low–high, with 1 indicating possibility that signal might be extracted if further filtering and/or different windowing to avoid noise before filter is applied.

Table T5. Expedition 340T vertical seismic profile (VSP) station quality and downhole location.

VSP station	Depth (*z*)		Good arrivals
	mbsl	mbsf	
1	1645	0	
2	1685	40	
3	1731	86	x
4	1745	100	x
5	1771	126	x
6	1795	150	x
7	1821	176	
8	1855	210	
9	1881	236	
10	1911	266	
11	1937	292	
12	1960	315	x
13	1990	345	x
14	2001	356	x
15	2027	382	x
16	2044	399	x
17	2067	422	
18	2089	444	x
19	2117	472	x
20	2145	500	
21	2175	530	x
22	2199	554	x
23	2222	577	x
24	2242	597	x
25	2269	624	
26	2294	649	x
27	2322	677	x
28	2347	702	
29	2380	735	x
30	2405	760	x
31	2433	788	x
32	2461	816	x
33	2480	835	x
34	2502	857	
35	2529	884	x
36	2557	912	x
37	2585	940	x
38	2610	965	x
39	2635	990	
40	2674	1029	x
41	2705	1060	
42	2735	1090	
43	2765	1120	
44	2791	1146	
45	2815	1170	x
46	2835	1190	
47	2861	1216	x
48	2888	1243	
49	2905	1260	x
50	2930	1285	x
51	2955	1310	
52	2979	1334	x
53	2994	1349	
54	3004	1359	
55	3005	1360	x

Figure F1. Atlantis Massif just west of the Mid-Atlantic Ridge spreading axis. Tectonic features, location of Hole U1309D (black circle), and seismic lines are indicated: white = MCS, dark gray = NOBEL deep source/ocean-bottom seismometer (OBS) refraction, light gray = traditional air gun/OBS refraction. Corrugations on domal core mark exposed detachment fault, well-mapped along south edge of the Southern Ridge and inferred from morphology and talc-schist fragments recovered in upper several meters (only) on Central Dome. Hanging wall block(s) are volcanic.

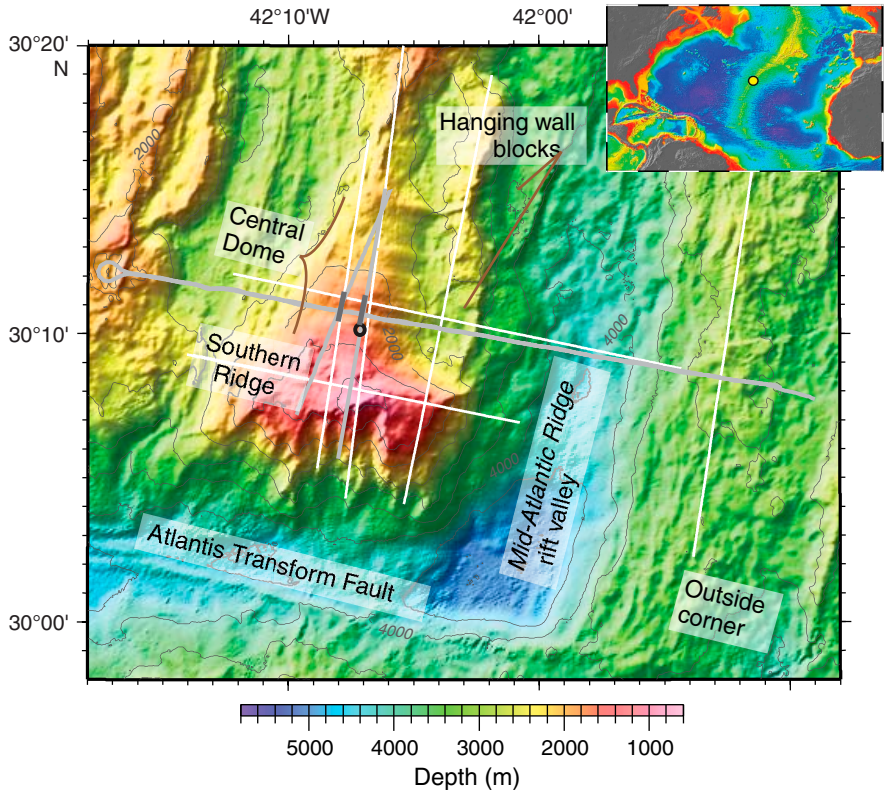

Figure F2. Multichannel seismic (MCS) data at Atlantis Massif. **A.** Migrated stack of Meg 10 across Central Dome (Canales et al., 2004). **B.** Unmigrated section (Singh et al., 2004) reveals a more complex band of wide-angle reflectivity starting at the D-reflector and extending ~0.5 s. Tomography model (Blackman et al., 2009) is overlain. **C.** Snapshots from Fledermaus scene show Singh wide-angle record sections and Hole U1309D lithology (depth converted to time using average check shot velocity). **D.** Velocity-depth profiles for near-bottom explosive source (NOBEL) (Collins et al., 2009), MCS refraction traveltime inversions (Canales et al., 2008), and sonic log from Hole U1309D overlain on envelopes of velocity determinations on other young Atlantic crust (yellow = Lucky Strike area [Arnulf, 2011]; gray = compilation, less resolution in shallow section [White et al., 1992]). TWT = two-way traveltime. CD = Central Dome, SR = Southern Ridge.

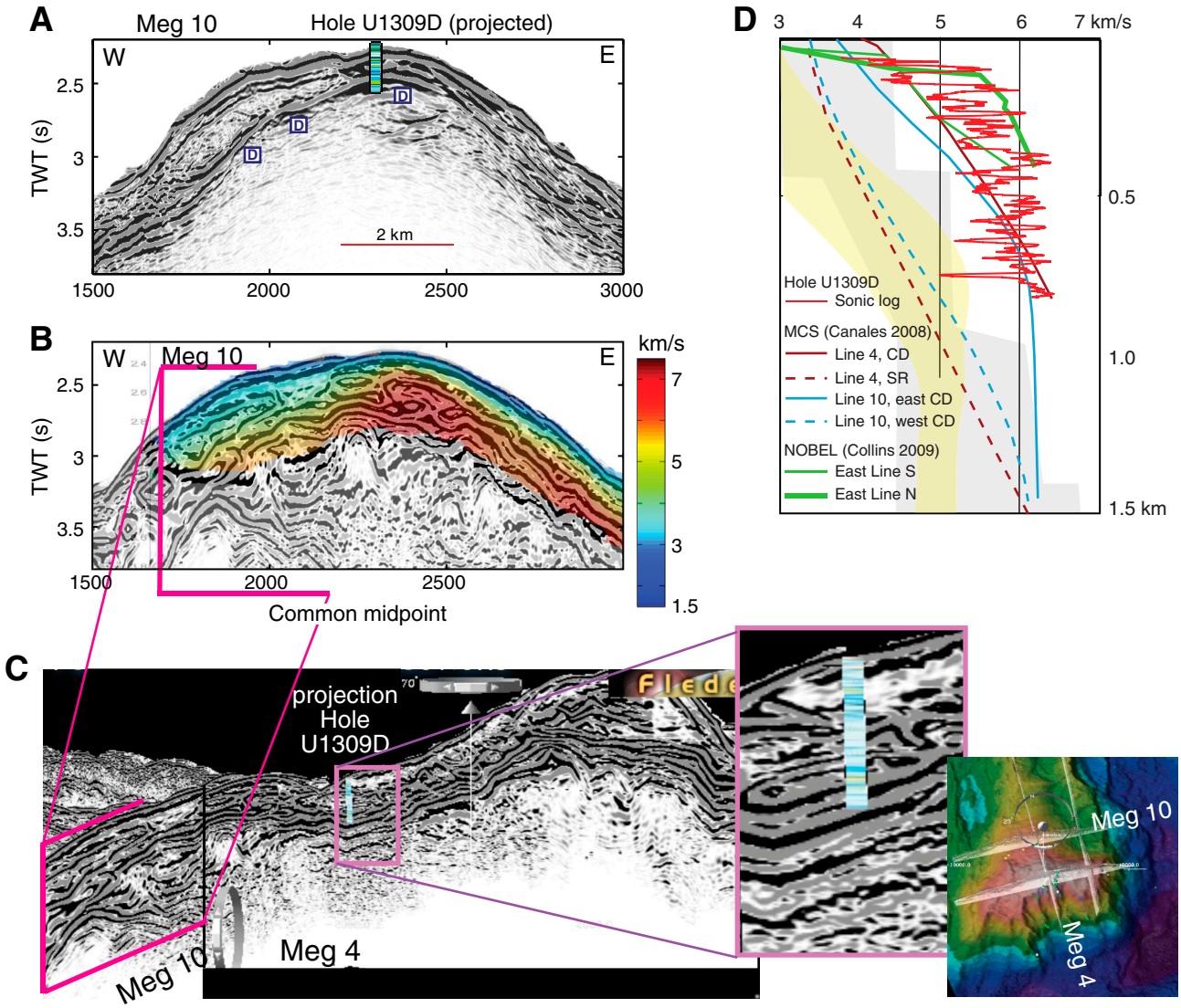

Figure F3. Downhole data obtained prior to Expedition 340T, Hole U1309D. **A.** Lithology is dominantly gabbroic with intervals of olivine-rich troctolite. **B.** Alteration of core pieces documented during Expedition 304/305 shipboard visual description. **C.** Density: red = logged, black dots = shipboard core sample. **D.** Logs of wall rock resistivity. **E.** *P*-wave velocity: red = log, black dots = core sample at room temperature/pressure. **F.** Expanded lithology in upper 800 m where seismic data existed prior to Expedition 340T.

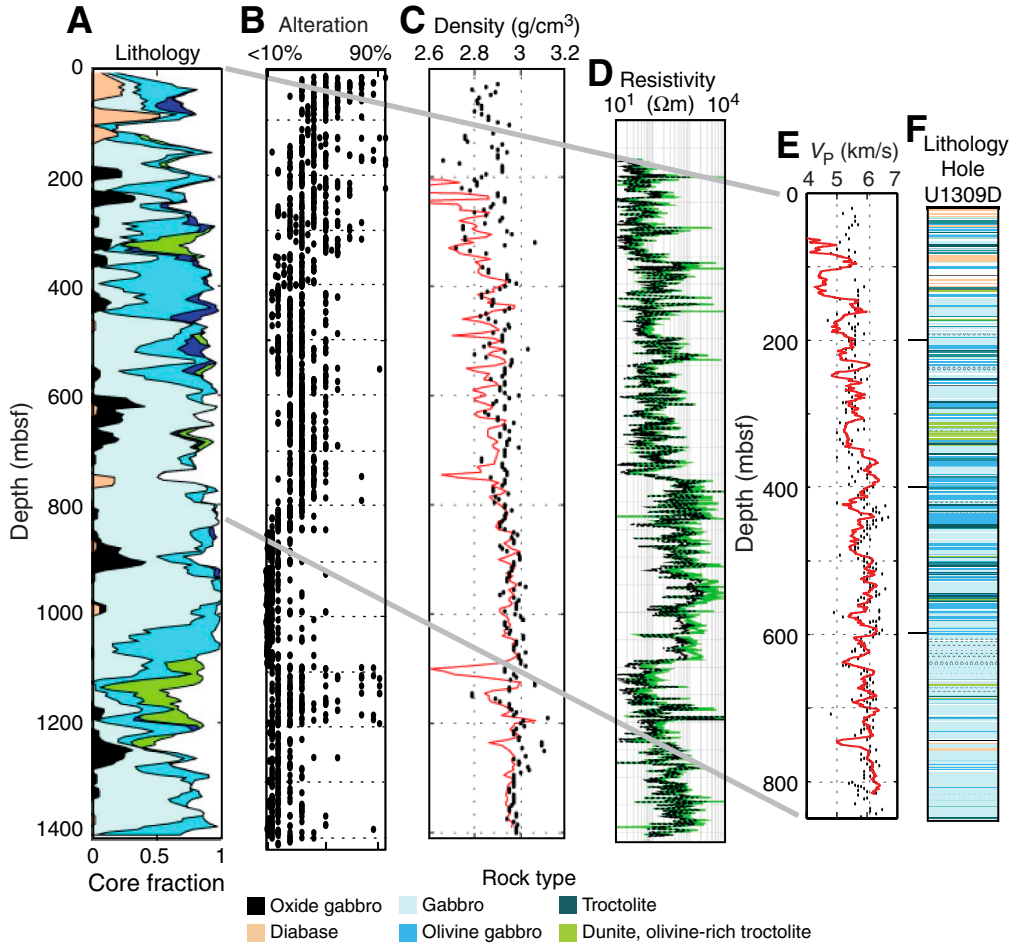

Figure F4. Wireline tool strings used during Expedition 340T. LEH-MT = logging equipment head–mud temperature, EDTC = Enhanced Digital Telemetry Cartridge, HLDS = Hostile Environment Litho-Density Sonde, HRLA = High-Resolution Laterolog Array, MTT = Modular Temperature Tool, DSI = Dipole Sonic Imager, GPIT = General Purpose Inclinometry Tool, VSI = Versatile Seismic Imager, MSS = Magnetic Susceptibility Sonde.

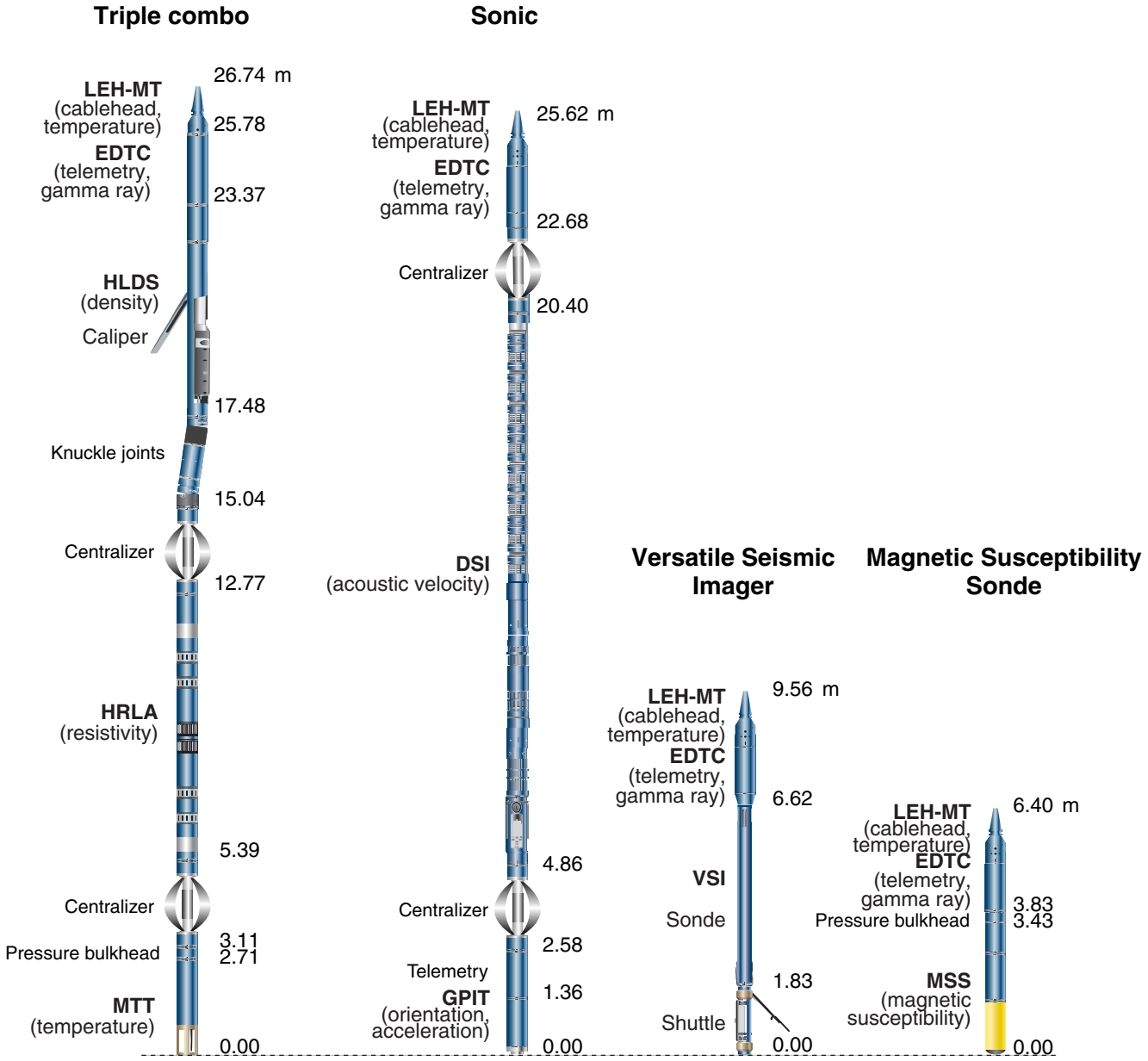

Figure F5. Map of Site U1309 (and Site U1392), showing Hole U1309D, where Expedition 340T logging was done, and Hole U1392A at Decoy mound, where a sample was obtained. Cyan track = approximate Expedition 340T camera survey locations, gray track = camera survey carried out during Expedition 304, when Holes U1309A–U1309E were drilled. The differences between locations targeted for offset Holes U1309A–U1309E are shown in comparison to position determined based on statistical ship position (reference point is Hole U1309D).

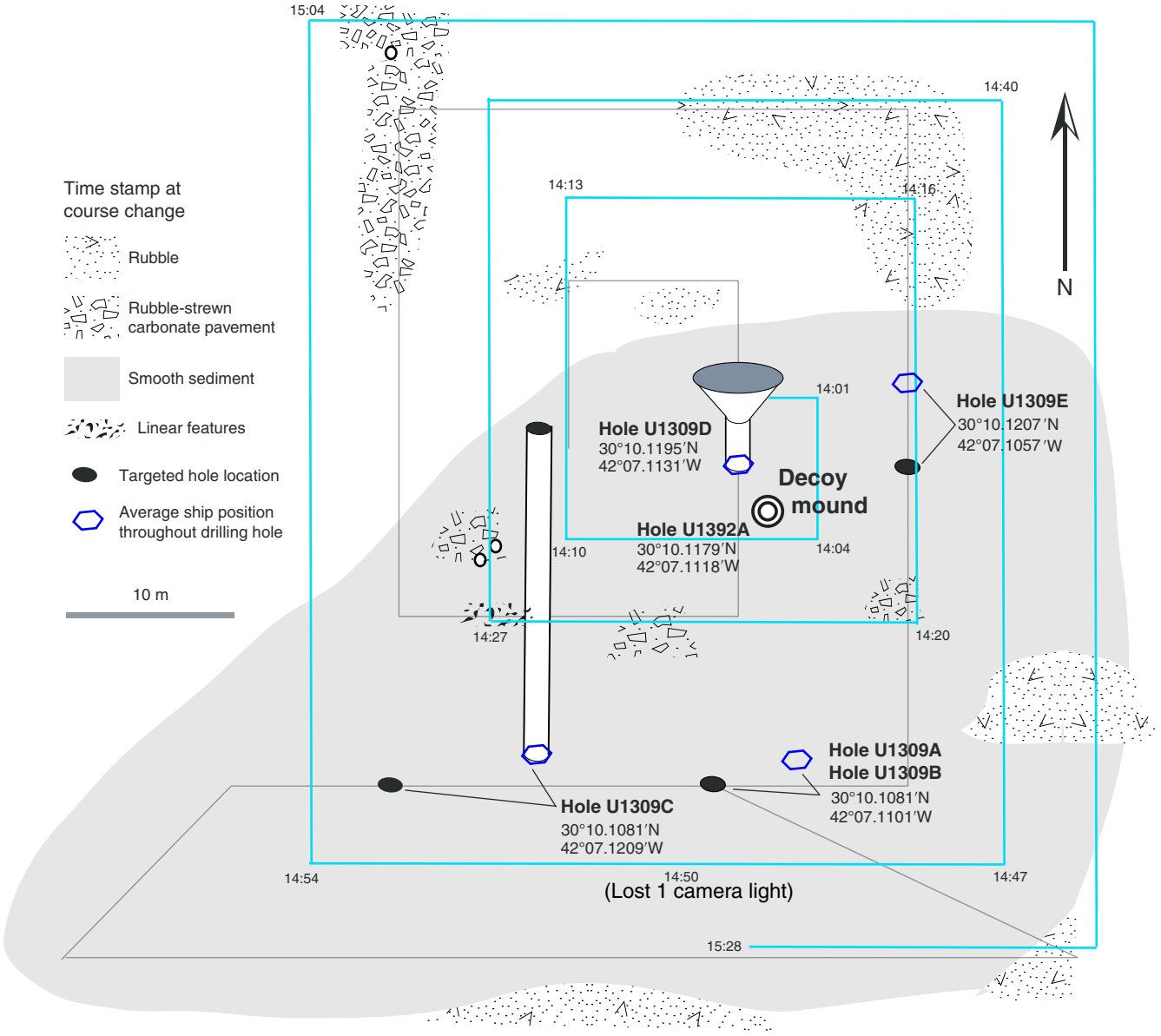

Figure F6. Summary of logs recorded during triple combo run, Hole U1309D. Hole size was measured by caliper of the HLDS. R5 = deepest resistivity reading of the HRLA, R3 = medium resistivity reading, RT = true resistivity, modeled from all depths of investigation. Temperature was measured by the MTT.

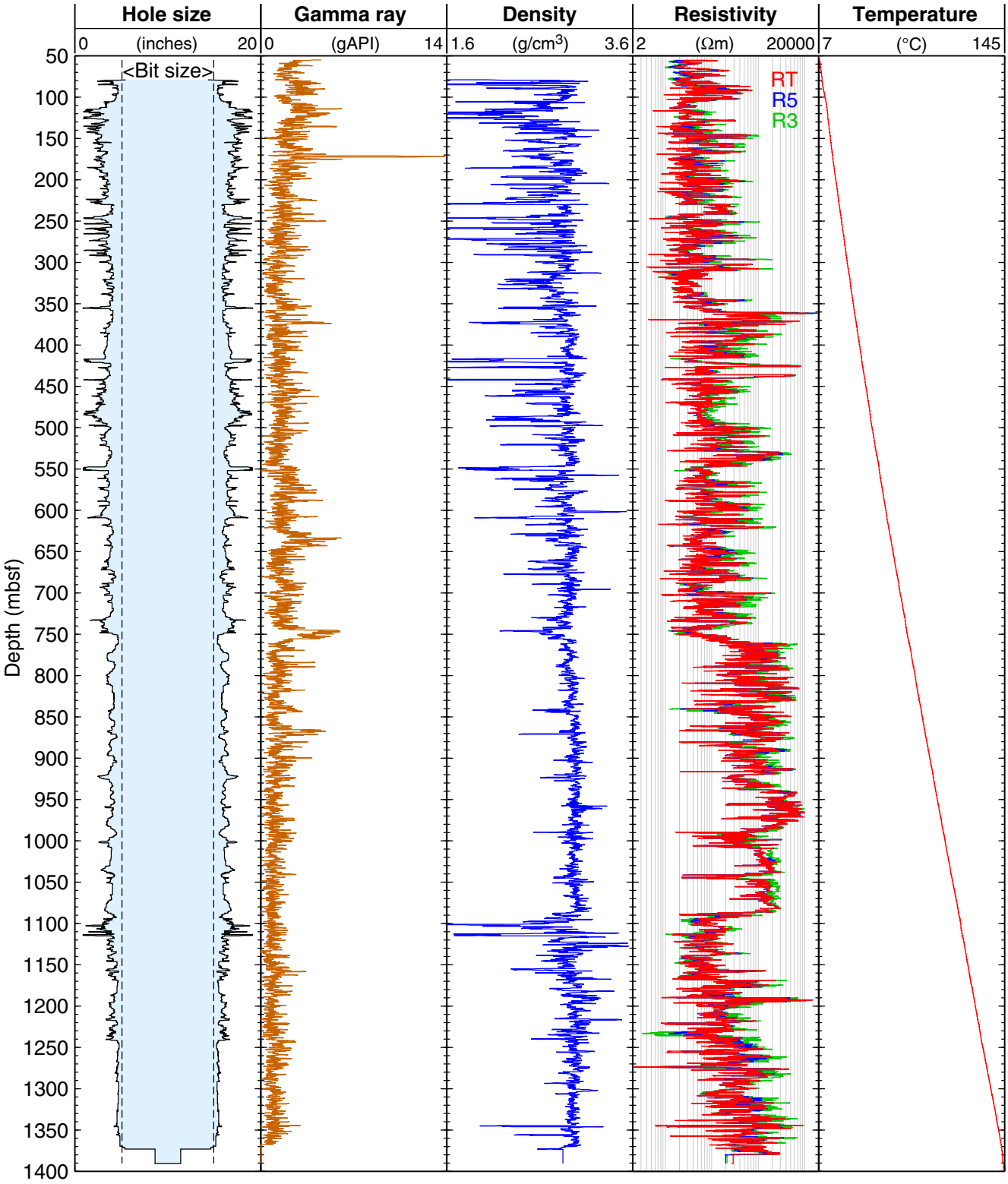

Figure F7. Summary of logs recorded by the sonic tool string, Hole U1309D, during Expedition 340T. Waveforms displayed are from DSI receiver closest to the transmitter. Coherence is measured across receivers and used to identify wave arrivals. HLDS = Hostile Environment Litho-Density Sonde. P = compressional arrival, S = shear arrival.

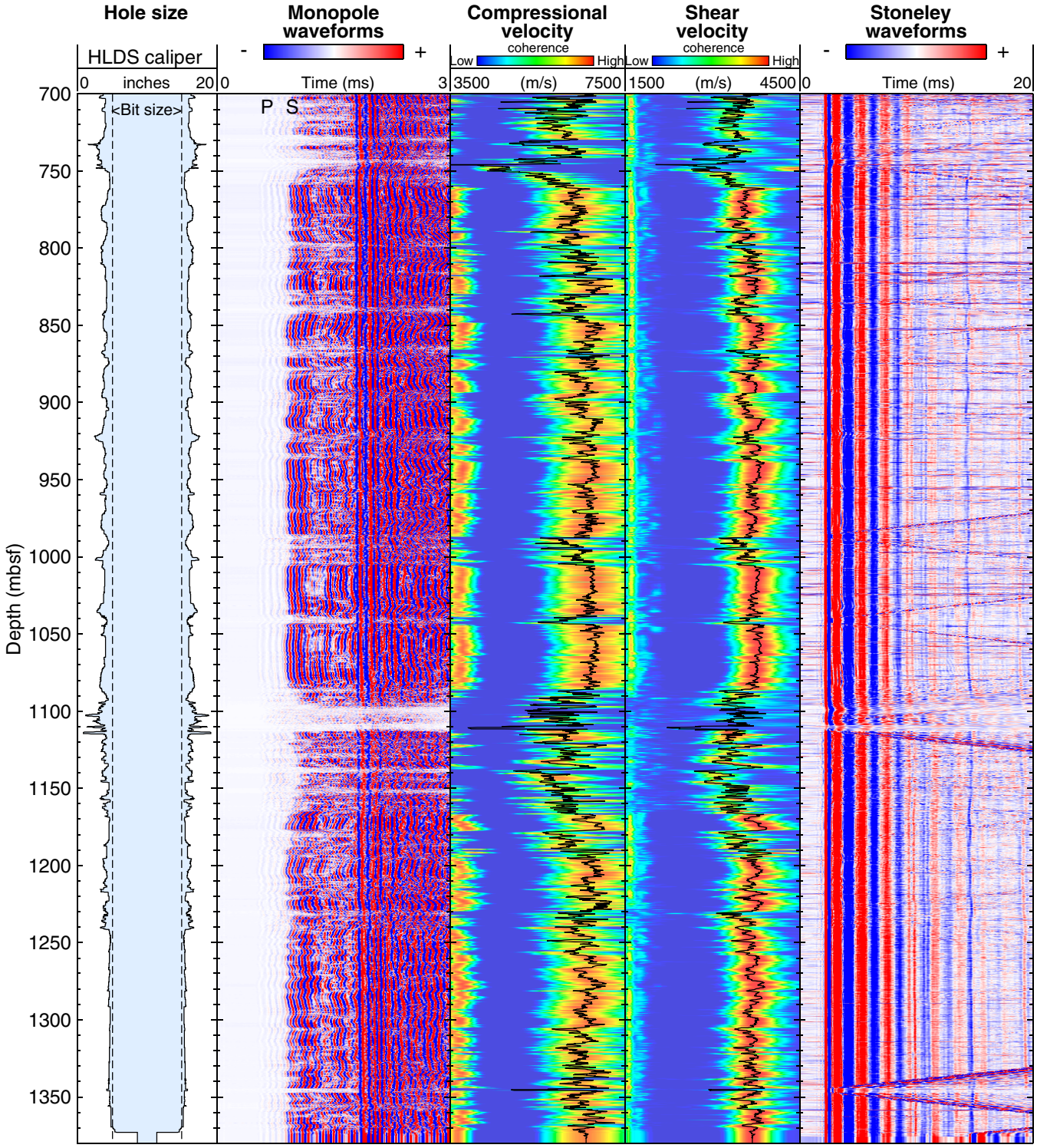

Figure F8. Comparison between logs recorded by Magnetic Susceptibility Sonde (MSS) string in Hole U1309D during Expedition 340T and magnetic susceptibility from the multisensor track (MST) on cores from Hole U1309D during Expedition 304/305.

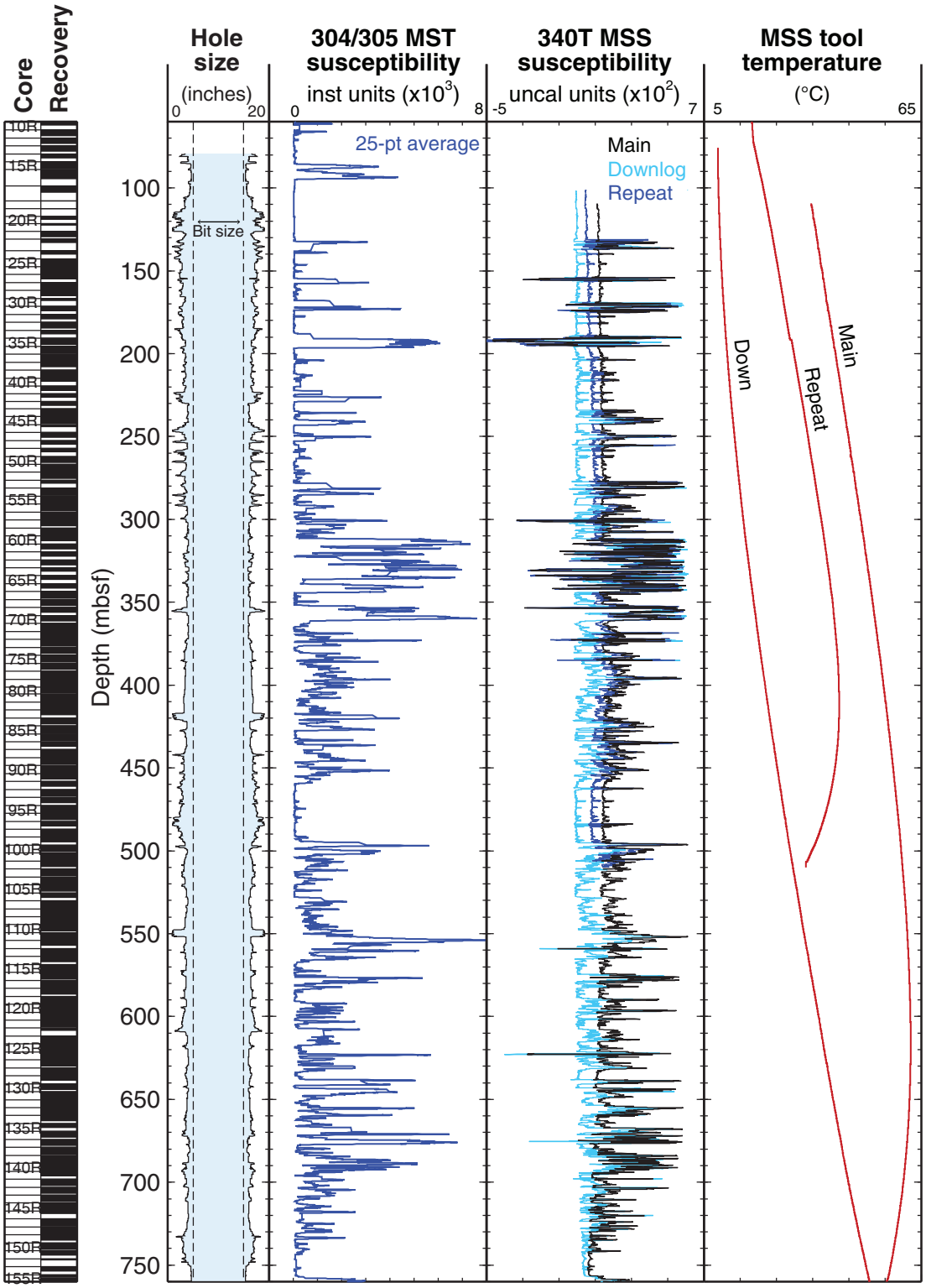

Figure F9. Comparison of the main logs recorded during Expeditions 305 and 340T. In the shallower section, the new data can be compared with some of the logs recorded during Expedition 304.

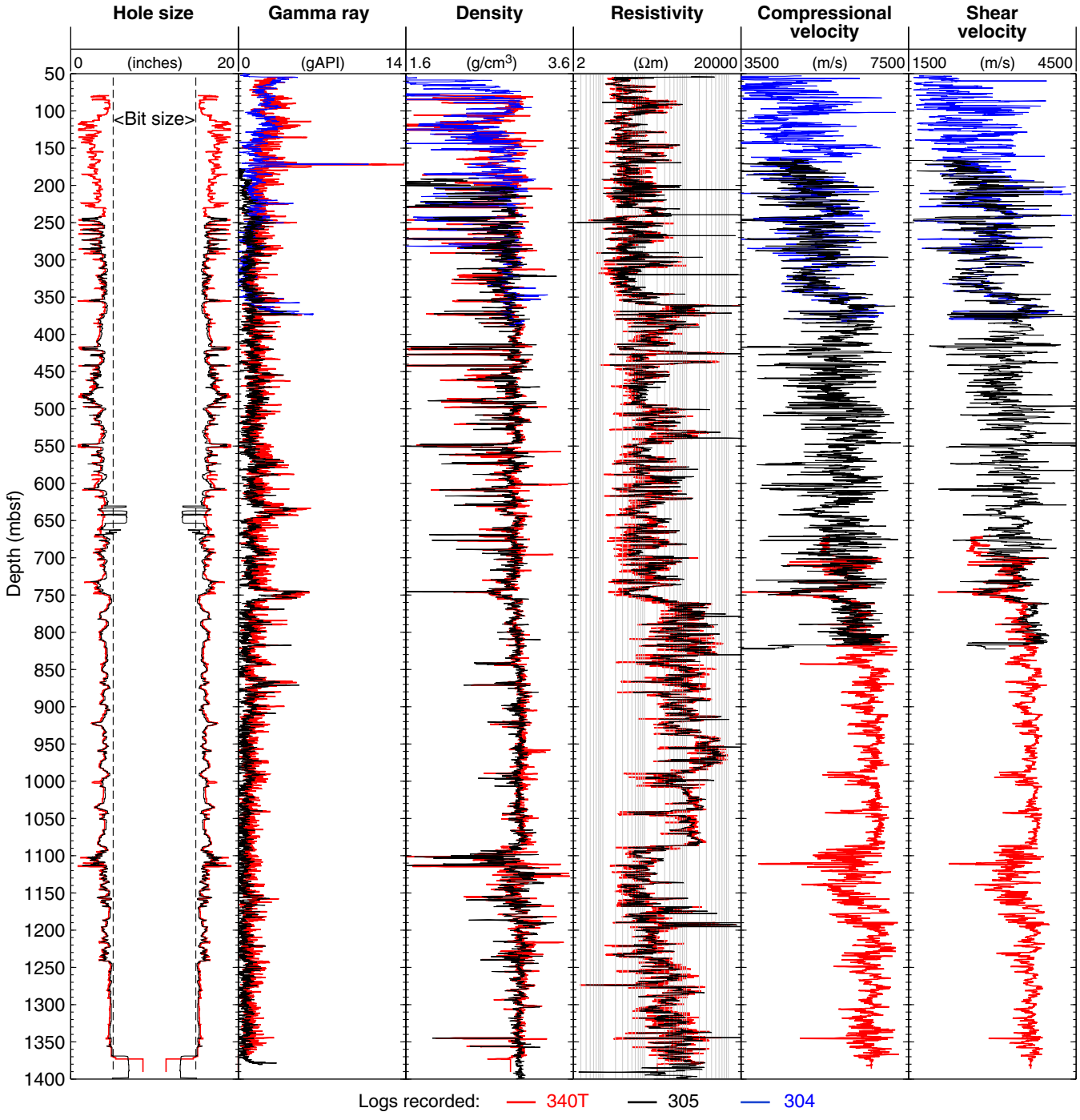

Figure F10. Temperature profile, Hole U1309D. Measured temperature during Expedition 340T triple combo logging run documents profile when disturbance of borehole fluid was minimal. Linear model (green dash) indicates some deviation from a simple conductive profile. Temperature at the end of Expedition 305 (black) was strongly affected by work in the hole. TAP = Temperature/Acceleration/Pressure, MTT = Modular Temperature Tool, LEH-MT = logging equipment head–mud temperature.

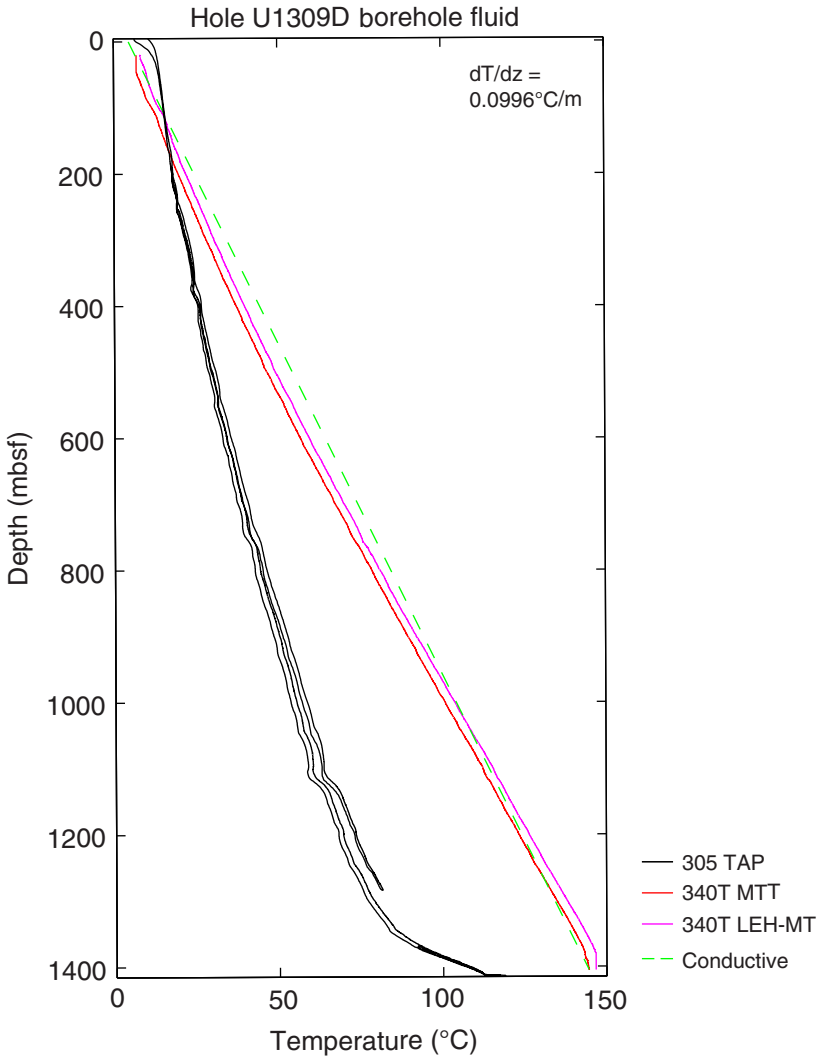

Figure F11. Velocity-depth profile for compressional waves in Hole U1309D and calculated vertical ray traveltimes. **A.** Black = MCS 3-D tomography model in Hole U1309D, red = running 10 m average of V_P data from Expeditions 304, 305, and 340T. **B.** Predicted vertical traveltime from rig floor to depth in the borehole based on sonic log data and tomography model. Dots = VSP station depths, pluses = stations with good data.

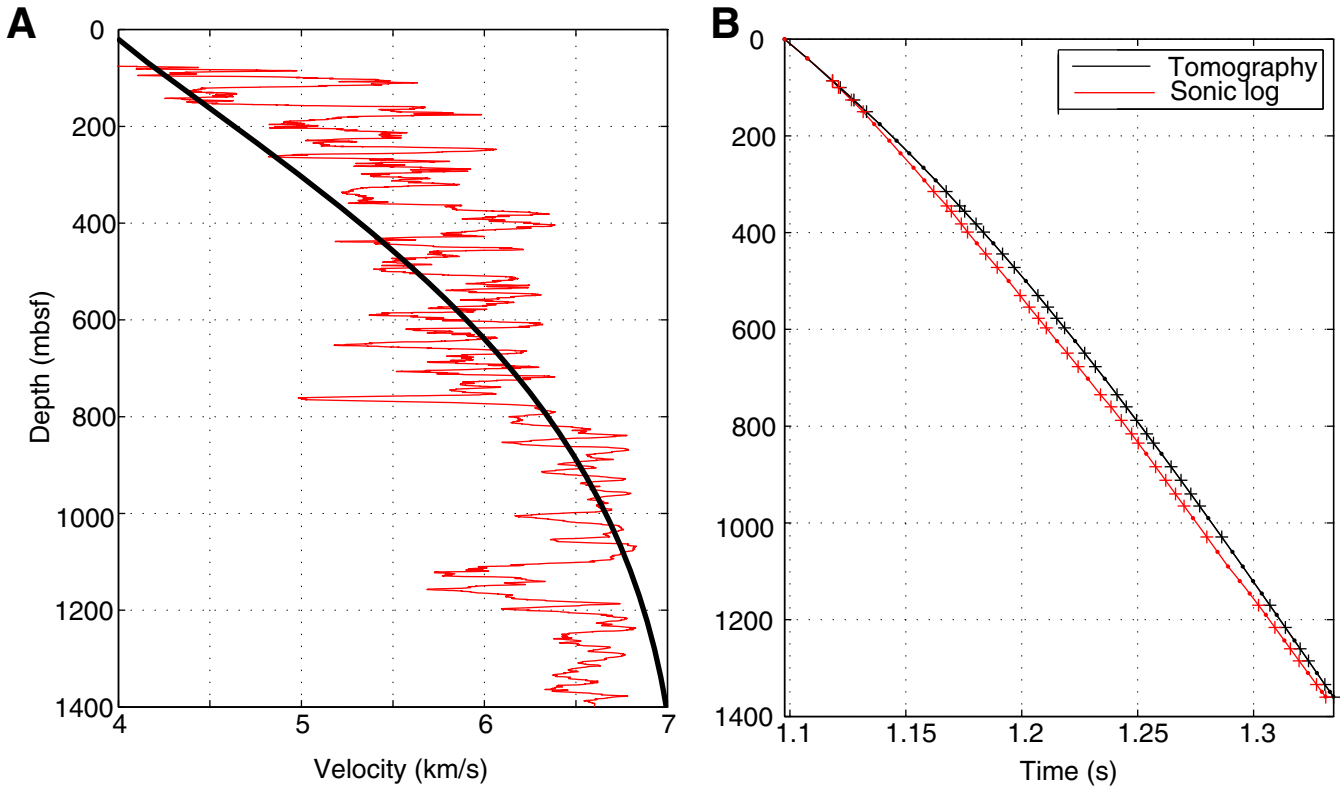

Figure F12. Example of high-quality VSP station data obtained during Expedition 340T, bandpass filter applied. Each of the triaxial VSI sensor components shows significant energy, indicating that *P*-wave is not vertically incident. Red star = predicted arrival time for this station at 150 mbsf.

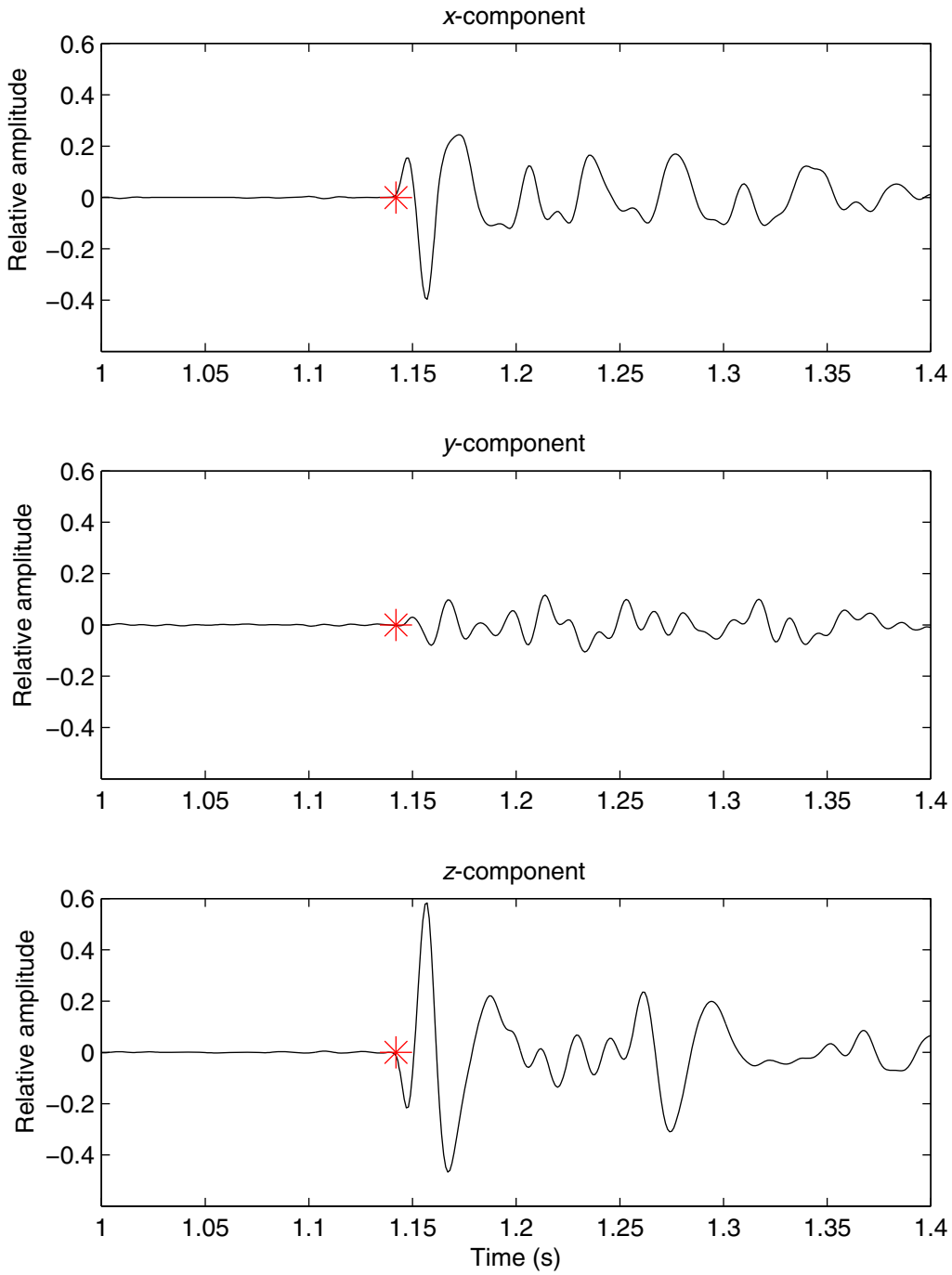

Figure F13. Example of very good trace quality recorded only on a single component for Expedition 340T VSP station at 1360 mbsf, bandpass filter applied. Red star = predicted arrival time for this source-receiver geometry.

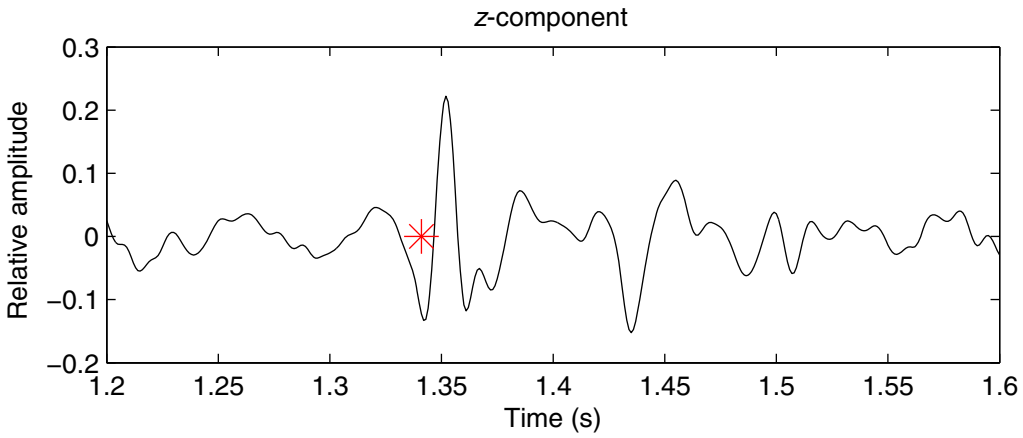

Figure F14. Identification of a fracture by energy reflected in Stoneley waveforms, Hole U1309D. Energy reflection is generated by a fracture that is seen at 1345.5 mbsf in FMS images recorded during Expedition 305.

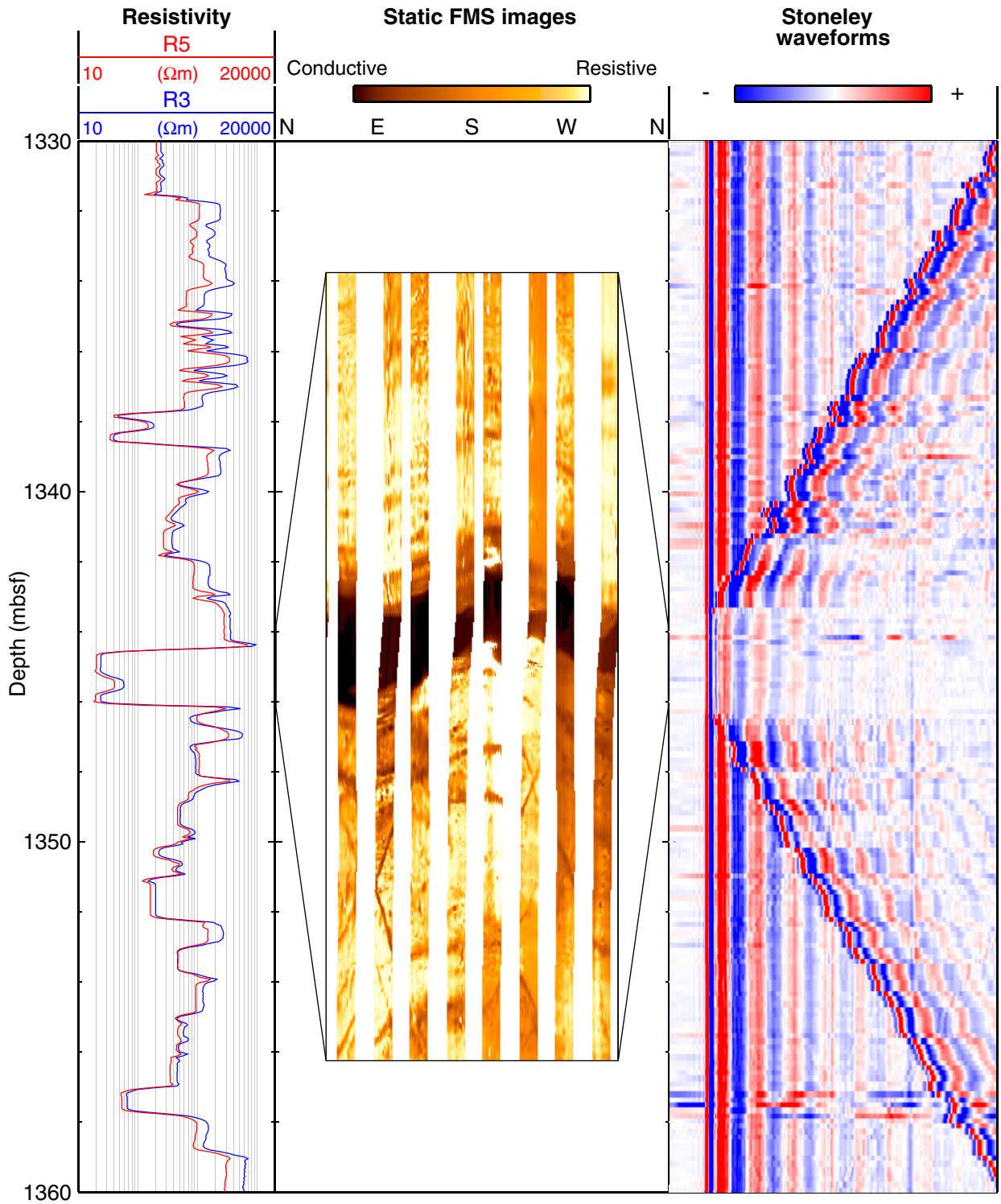

Figure F15. Comparison of core lithology with magnetic susceptibility from Expedition 340T logging data (Magnetic Susceptibility Sonde [MSS]) and Expedition 304/305 core pieces (multisensor track [MST]) (25 point running average). Yellow bands highlight intervals where good correlation is observed between the two data sets. Distinctive features in magnetic susceptibility from logs and cores correspond to serpentinized intervals and oxide gabbro intervals.

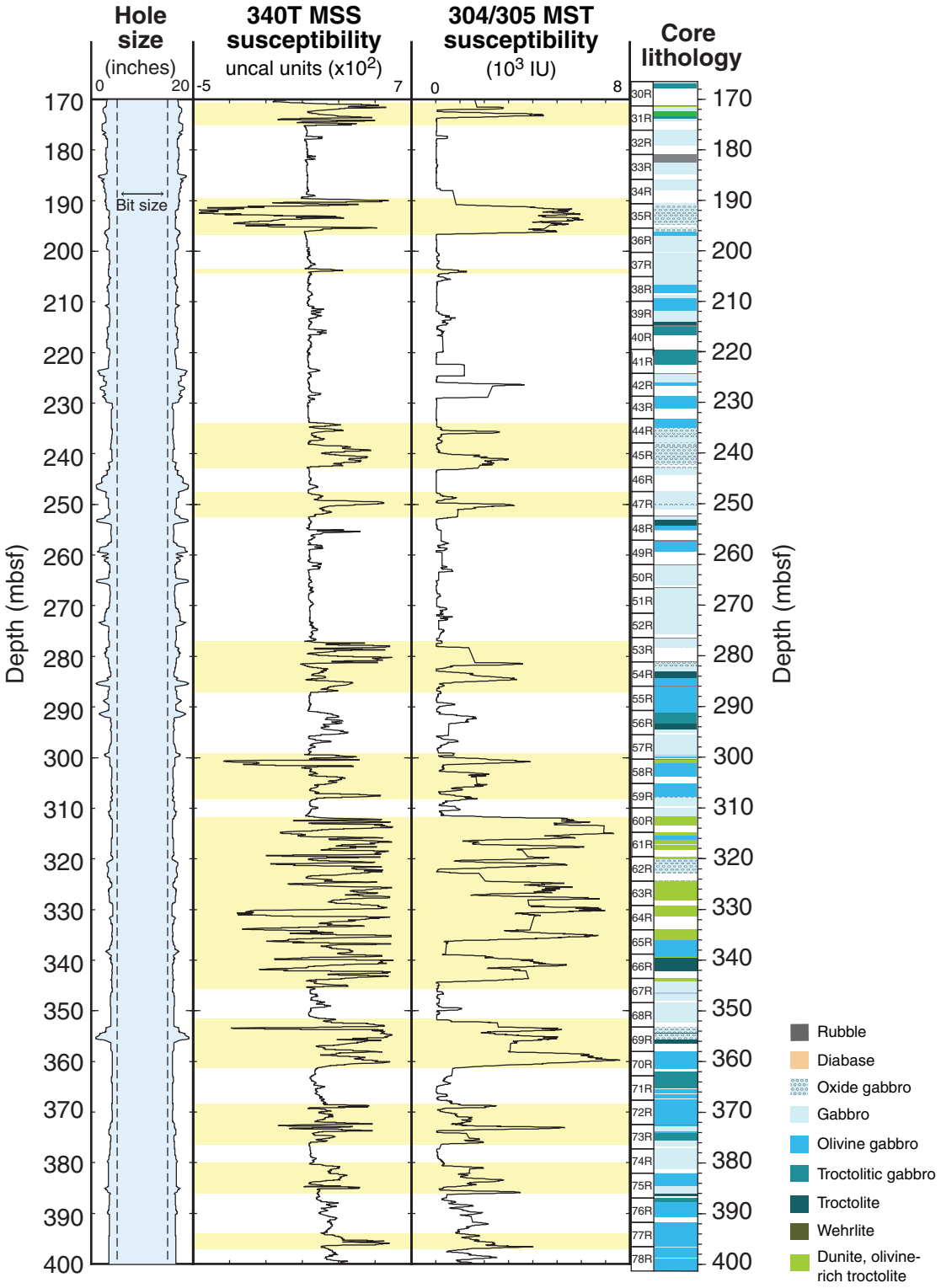

Figure F16. VIT video frame captures of "Decoy" mound. Distinct outer wall has irregular shape, characteristic of a precipitation deposit. Diameter of this structure is ~2 m. Logging bit approached, pushed in, and met impenetrable interface within 1–2 m. Hole U1309D reentry cone (lower left), just a few meters away from Decoy mound, shows little sediment accumulation since Expedition 305 departed 7 y ago.

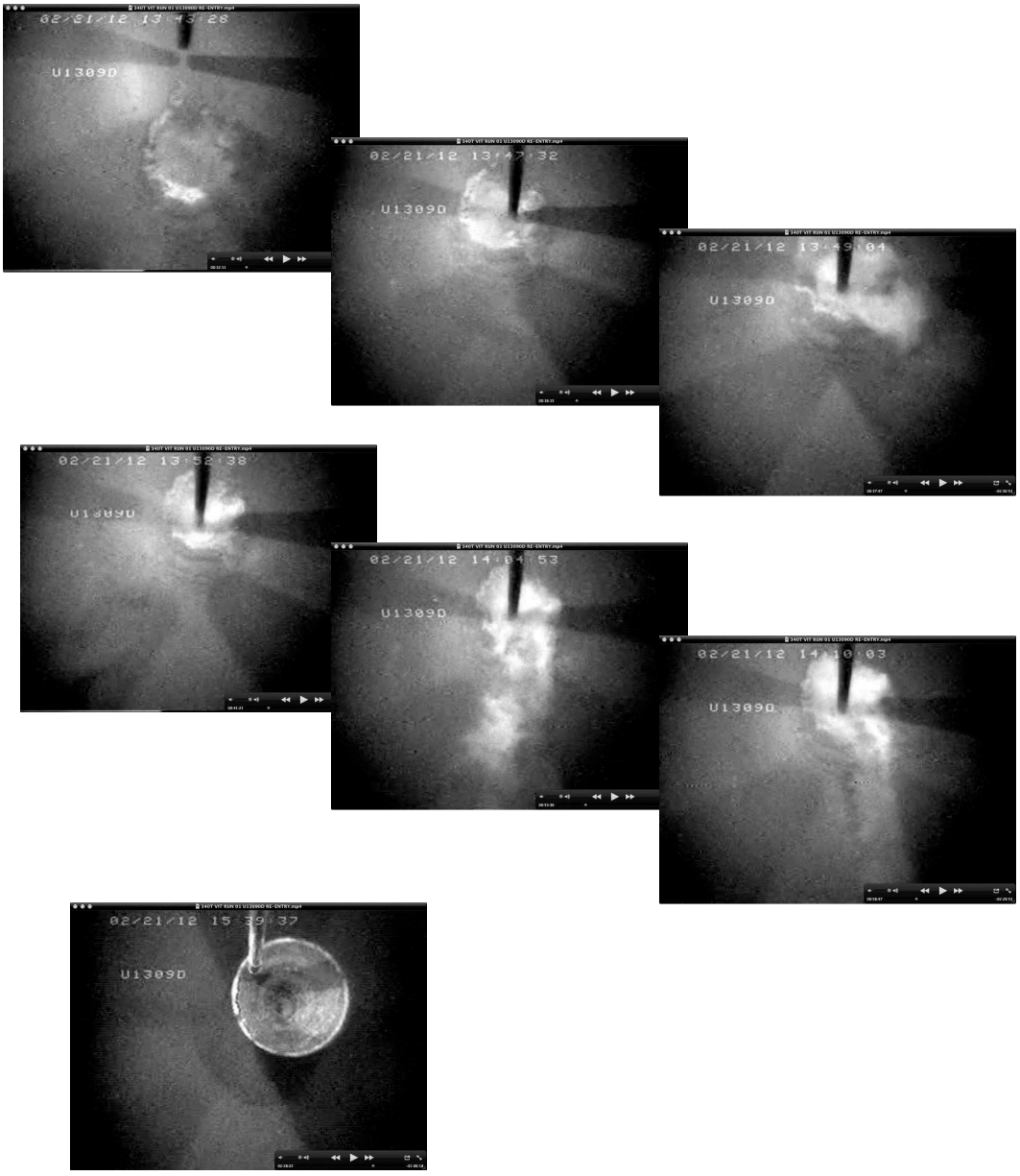

Figure F17. Photos of Sample 340T-U1392A-1M-CC. **A.** Complete sample. **B.** Platy black fragments: top = black face of fragments, middle = close-up of striations on black face, bottom = rust-colored side. **C.** Close-up of possible fault rock fragments. **D.** Single larger lithified carbonate piece (also visible as light pebble near center of A) and a close-up of another piece. **E.** Representative view of rock fragments that make up a majority of the sample with a few microfossils.

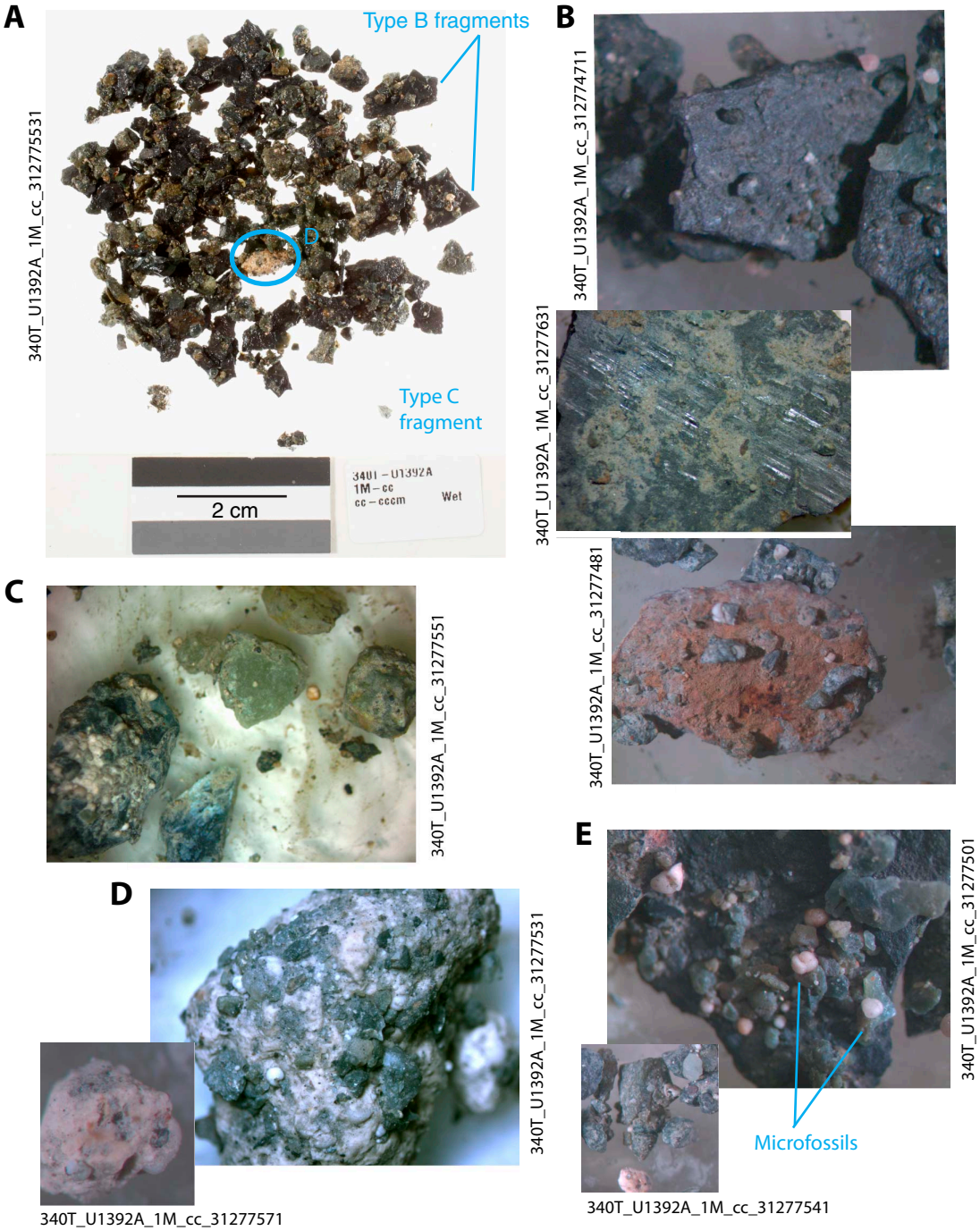

Figure F18. Correlation of downhole sonic velocity and lithology. V_P shown for each of the Hole U1309D logging phases (blue = Expedition 304, cyan = Expedition 305, red = Expedition 340T. Scale at bottom). Green = V_P/V_S ratio for all three logging runs (scale at top).

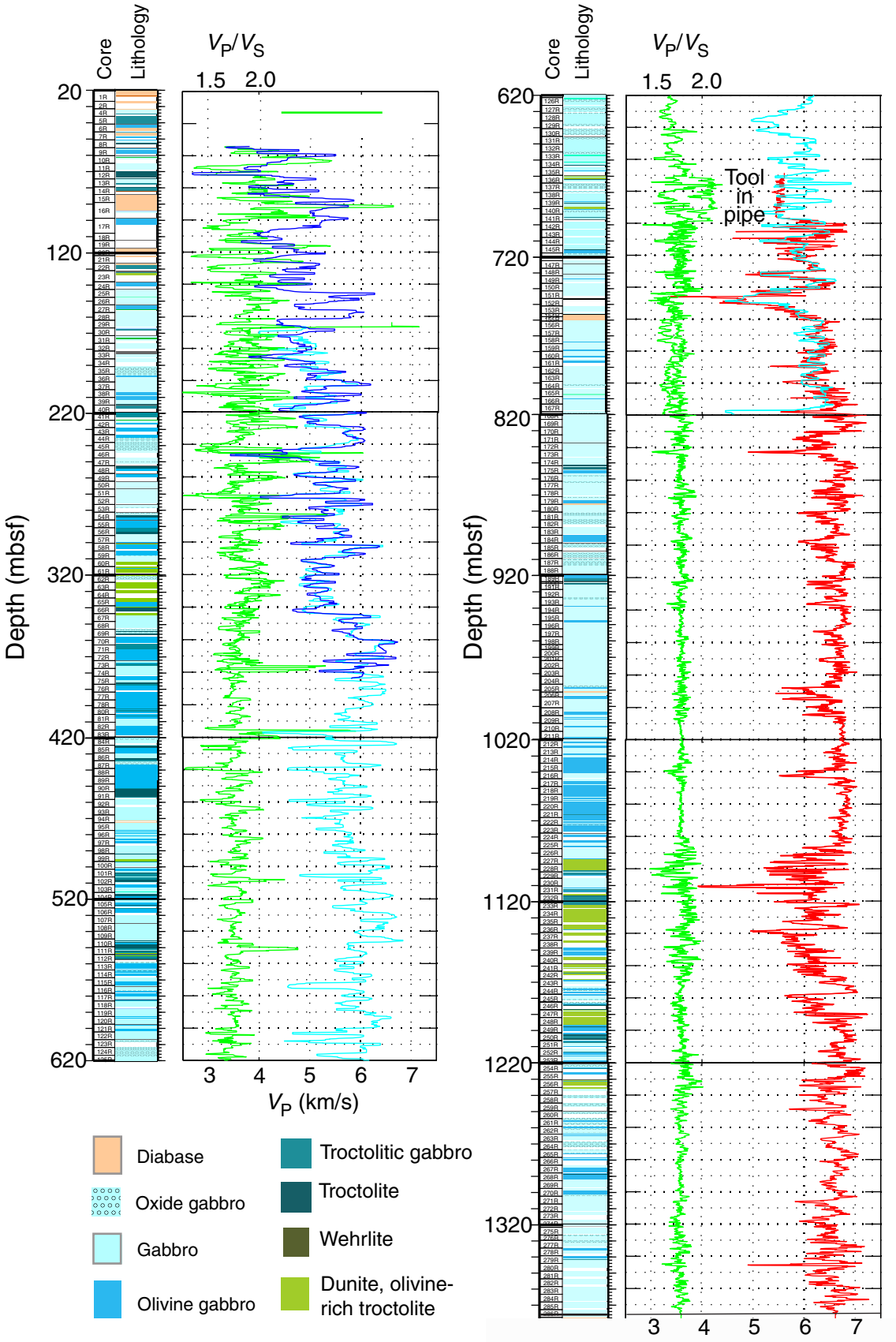

Figure F19. Downhole lithology in Hole U1309D (20 m average) and location of vertical seismic profile (VSP) stations determined to have useful data. Red dots = Expedition 340T stations, black dots = Expedition 305 stations.

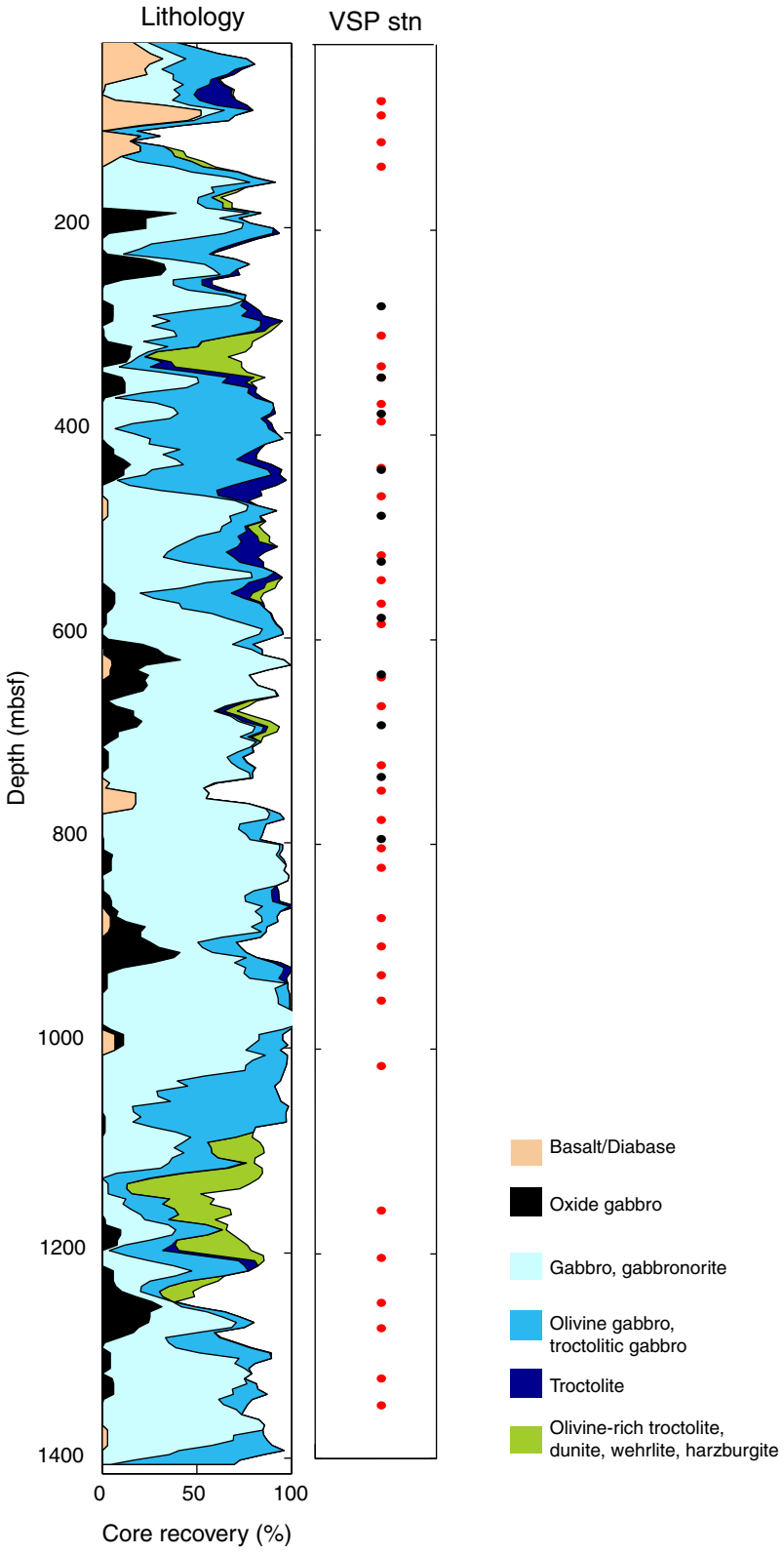

Figure F20. Correlation of downhole temperature (*T*), lithology, and structure, Hole U1309D. **A.** Deviation of Expedition 340T temperature from simple conductive model. **B.** Core lithology. **C.** Crystal-plastic deformation structures observed in Hole U1309D core. Intensity scale: 0–5 (low–high). **D.** Cataclastic structures observed in Hole U1309D core. Dashed horizontal lines = locations of fazones (FZ) inferred from core structure and, in some intervals, Expeditions 304/305 logging data.

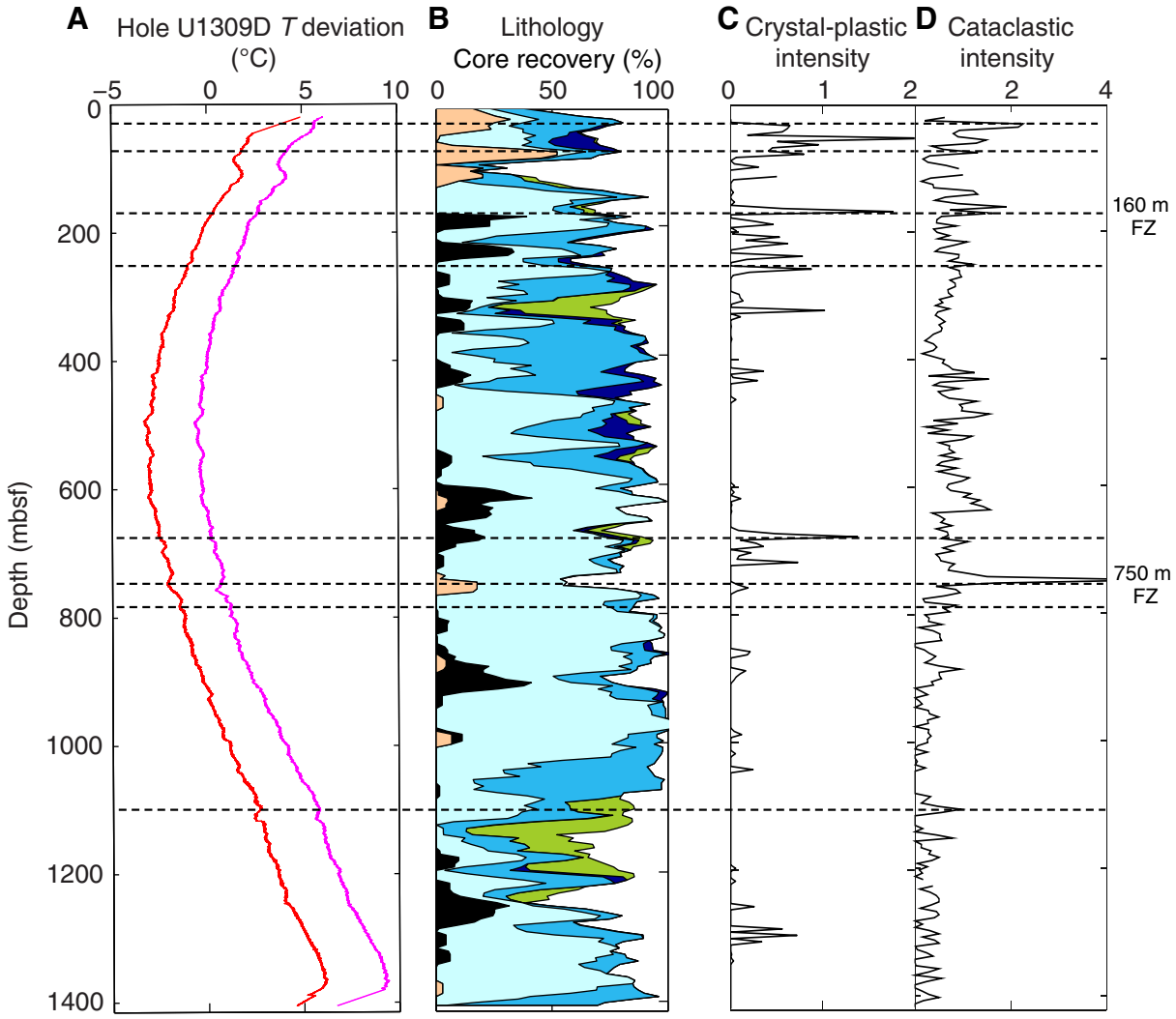

Appendix

Matlab scripts

The Matlab scripts in this section were used to make a preliminary assessment of data quality from the Expedition 340T VSP. The scripts present time-windowed and band-pass filtered versions of all sensor components, shot-by-shot, for a single VSP station. The window is a short time interval based upon time integration of a 1-D velocity model for the hole (see **"Principal results"**). Time integration of the sonic log data gives essentially the same predictions. The main script is **"cull_vsp_data."** It uses **"rdsegy_full"** to ready the SEGY versions of the VSP data and **"butter_filt"** to apply a band-pass Butterworth causal filter.

cull_vsp_data

```
% CULL_VSP_DATA - script to go through 3 component VSP data with traces
% selected by station ID and plot all components for all shots at a given station
% depth one shot at a time.
% The VSP data from Expedition 340T was sufficiently noisy that arrivals could
% only be identified by focusing on a short time window centred on the expected
% arrival time and comparing filtered and unfiltered versions of the traces of
% a shot
%
% Shot-to-shot variability was high enough that displaying all traces for all
% shots at a single station was not feasible.
%
% Based on this display a initial data quality assessment was made for shots
% from the 340T VSP.
%
% Required files
%       SEG-Y files with x,y & z data
%       Station text file with 3 columns station ID, depth (m), predicted time(s)
% a. j. harding

stationFile = 'vsp_time_pred.txt';  %  3 column table of predicted arrival times

vspDir  = '../Expedition_340T/data/vsp';  % Directory with SEG-Y data
xFile = '340T-U1309D_raw_shot_geo_x.segy';  % Actual files
yFile = '340T-U1309D_raw_shot_geo_y.segy';
zFile = '340T-U1309D_raw_shot_geo_z.segy';

              % Length of time display window relative to time precition
windowB = 0.1;    % before pick
windowT = 0.2;    % after  pick

time_pred_offset = 0.010;  % Adjustment of prediction for gun delay, gun depth etc.

            % Read VSP station file with IDs, depths & time prediction
data = load(stationFile);
```

```
station_id    = data(:,1);
station_z     = round(data(:,2)*1000);  % convert m
station_tpred = data(:,3);

max_ID = max(station_id); % Maximum station #

if ~exist('seisz','var')
  [seisz,header] = rdsegy_full(fullfile(vspDir,zFile));
  seisx = rdsegy_full(fullfile(vspDir,xFile));
  seisy = rdsegy_full(fullfile(vspDir,yFile));

  ixDepth = find(header.lactive == 11);   % Row with station elevation wrt sea level

  ixScalar = find(header.sactive == 35);  % Scalar for elevation
  elevScalar = double(header.short(ixScalar,1));  % Assume it doesn't change
  if elevScalar < 0; elevScalar = -1/elevScalar; end

  ixSampRate = find(header.sactive == 59);
  dt  = double(header.short(ixSampRate,1))/1000000.; % convert from INT16
end

          % Set up parameters for Butterworth low/highpass filtering
fc = [10,60];    % corner frequencies in Hz
[Bl,Al] = butter_filt(4,fc(2),dt,'low');  % 4-pole low
[Bh,Ah] = butter_filt(3,fc(1),dt,'high'); % 3-pole high

          % Read in the 3 components of data & header information
          % Only do this once per session

nt = size(seisz,1);        % samples
ntotal = size(seisz,2);    % # of shots/traces

tv = [0:nt-1]*dt;    % time vector for x-axis of plot

         % Apply filters as two part cascade low then high
filt_seisx = filter(Bl,Al,seisx);
filt_seisy = filter(Bl,Al,seisy);
filt_seisz = filter(Bl,Al,seisz);

filt_seisx = filter(Bh,Ah,filt_seisx);
filt_seisy = filter(Bh,Ah,filt_seisy);
filt_seisz = filter(Bh,Ah,filt_seisz);

       % Use depth from SEG-Y header to assign station IDs to all shots
       % used to select data for plotting.
       % NOTE must convert to double from INT32
zdata = -double(header.long(7,:))/10000.; % Station depths from segy headers

station_data = ones(ntotal,1);
for j = 1:ntotal
  ik = find(abs(station_z - zdata(j)) < 0.5);
  station_data(j) = station_id(ik);
end
```

```
while(1)
  curStation = input('Enter current station (<=0 to finish) ');

  if (curStation > max_ID); continue; end
  if (curStation <= 0); break; end

             % Extract station depth & travel time prediction
  ixcur   = find(station_id == curStation);

  curZ = station_z(ixcur);
  curT = station_tpred(ixcur) + time_pred_offset;

               % Calculate sliding window around time prediction
  tbeg = floor((curT-windowB)/0.1)*0.1;
  tfin =  ceil((curT+windowT)/0.1)*0.1;

  ixb = round(tbeg/dt)+1;
  ixt = round(tfin/dt)+1;

  ixRange = [ixb:ixt];

                % Select traces for the current station

  ixselect = find(station_data == curStation);

  nselect = length(ixselect);

  tv_loc = tv(ixRange);

  xTraces =  seisx(ixRange,ixselect)';
  yTraces =  seisy(ixRange,ixselect)';
  zTraces =  seisz(ixRange,ixselect)';

  fxTraces = filt_seisx(ixRange,ixselect)';
  fyTraces = filt_seisy(ixRange,ixselect)';
  fzTraces = filt_seisz(ixRange,ixselect)';

         % Create clipped version of traces
  clipAmp = 1.;

  ixClip = find(abs(fxTraces(:)) > clipAmp);
  cxTraces = fxTraces;
  cxTraces(ixClip) = NaN;

  ixClip = find(abs(fyTraces(:)) > clipAmp);
  cyTraces = fyTraces;
  cyTraces(ixClip) = NaN;

  ixClip = find(abs(fzTraces(:)) > clipAmp);
  czTraces = fzTraces;
  czTraces(ixClip) = NaN;

           % Now loop through traces plotting 3 windows
```

```
        %   Unfiltered data - autoscaled by Matlab
        %   Filtered  -  data also autoscaled
        %   Clipped  - y axis will be no larger than clipAmp
for j = 1:nselect
  titleString = sprintf('x Comp Station: %d at z: %d Trace %d', ...
                                    curStation,curZ,ixselect(j));

  figure(1)      % Unfiltered
    clf

    subplot(3,1,1)
      plot(tv_loc, xTraces(j,:),'k');
      hold on
      plot(curT,0,'*r','markerSize',13);  % time prediction
      xlim([tv_loc(1),tv_loc(end)]);
      title(titleString)

    subplot(3,1,2)
      plot(tv_loc, yTraces(j,:),'k');
      hold on
      plot(curT,0,'*r','markerSize',13);
      xlim([tv_loc(1),tv_loc(end)]);
      title('y Component');

    subplot(3,1,3)
      plot(tv_loc, zTraces(j,:),'k');
      hold on
      plot(curT,0,'*r','markerSize',13);
      xlim([tv_loc(1),tv_loc(end)]);
      title('z Component');

  figure(2)    % Filtered
    clf
    subplot(3,1,1)

      plot(tv_loc,fxTraces(j,:),'k');
      hold on
      plot(curT,0,'*r','markerSize',13);
      xlim([tv_loc(1),tv_loc(end)]);
      title(titleString)

    subplot(3,1,2)
      plot(tv_loc, fyTraces(j,:),'k');
      hold on
      plot(curT,0,'*r','markerSize',13);
      xlim([tv_loc(1),tv_loc(end)]);
      title('y Component');

    subplot(3,1,3)
      plot(tv_loc, fzTraces(j,:),'k');
      hold on
      plot(curT,0,'*r','markerSize',13);
      xlim([tv_loc(1),tv_loc(end)]);
      title('z Component');
```

```
    figure(3)    % clipped
      clf
      subplot(3,1,1)
        plot(tv_loc,cxTraces(j,:),'k');
        hold on
        plot(curT,0,'*r','markerSize',13);
        xlim([tv_loc(1),tv_loc(end)]);
        title(titleString)

      subplot(3,1,2)
        plot(tv_loc, cyTraces(j,:),'k');
        hold on
        plot(curT,0,'*r','markerSize',13);

        xlim([tv_loc(1),tv_loc(end)]);
        title('y Component');

      subplot(3,1,3)
        plot(tv_loc, czTraces(j,:),'k');
        hold on
        plot(curT,0,'*r','markerSize',13);
        xlim([tv_loc(1),tv_loc(end)]);
        title('z Component');

      pause  % Wait for user to press key to continue
  end   % for nselect
end  % while
```

rdsegy_full

```
function [seis,header,binh] = rdsegy_full(fname)
% RDSEGY_FULL returns both SEG-Y data and a header structure with active entries
%
%  [seis,header,binh] = rdsegy_full(fname)
%
%
% Inputs
%    fname: input file name
%
% Outputs:
%    seis[nsamps, nx]: Seismogram data
%    header - structure containing active header entries from the trace
%             header (defined as a non-zero value for any trace).
%       .sactive - indices in header of active short integer entries
%       .lactive -   "      "   "         "     long   "      "
%       .short(nactiveS,nx) - matrix with short header entries
%       .long(nactiveL, nx) - matrix with long  header entries
%
%  a. j. harding, March 2012

       % Indices for elements of the SEGY trace header
insamp = 58; % Header number of samples
```

```
      %   Open file and position past the EBCDIC header
fid = fopen(fname, 'r','ieee-be');
if fid == -1
   error('*** RDSEGY_FULL *** Error opening seismogram file')
end

fseek(fid,0,1);
totalBytes = ftell(fid);
                % Skip over the EBCDIC Header
fseek(fid,3200,-1);

      % Read the Binary header & check data format
      % The data format is stored in element 13 of the binary header. By
      % convention Sioseis denotes data in host machine floating point format
      % with an ID >= 5. This routine assumes floating point format and does
      % format conversion

binh = fread(fid,200,'short');

data_format = binh(13);

switch data_format

case 1 % IBMFP
  disp('Format is IBM fp')
  form_str = 'uint';
  form_str = 'float32';
  data_size_bytes = 4;

case 2
 form_str = 'int32';
 data_size_bytes = 4;

case 3
 form_str = 'int16';
 data_size_bytes = 2;

case 5          % Native floating point
 form_str = 'float32';
 data_size_bytes = 4;

otherwise
  fprintf(2,'RDSEGY2 BINARY HDR Cannot read data format\n');
  fprintf(2,'Data format %d\n',data_format);
  error('**EXIT**');
end

disp('***WARNING*** forcing format to native floating point');
form_str = 'float32';
data_format = 5;

     % Read the 1st header to find the no. of samples/trace
T1 = fread(fid,120,'short')';
```

```
nsamps = T1(insamp);

fseek(fid,-240,0);

       % Estimate total number of traces from no. of samples
ntrEst = (totalBytes - 3600)/(240+nsamps*data_size_bytes);

      % Preassign an initial storage space for trace headers/data.
      % (Preassignment significantly increases read speed)
      % The header for each trace is read twice and once as short ints and
      % once as long ints, thus there are 2 header buffers ibuf & lbuf.

ntr = max(1000,ntrEst); % Size of buffer increments
ibuf = zeros(120,ntr);
lbuf = zeros( 60,ntr);
%bseis = zeros(nsamps,ntr);

seis = zeros(nsamps,ntr);

              % >>>>>>>> Main Reading Loop : Read all traces <<<<<<<<

nx =  0; % Number of traces read

tic
while (1)
  T1 = fread(fid,120,'int16');

  if (feof(fid) == 1) break; end

  nsamps = T1(insamp);

  fseek(fid,-240,0);
  T2 = fread(fid,    60,'int32');

  T3 = fread(fid,nsamps,form_str);   % read trace data
  if data_format == 1;
    T3  = ibm2num(uint32(T3));
  end

  nx = nx + 1;
                % Allocate additional storage space for data arrays
  if (rem(nx,ntr) == 1 & nx > 2)
    seis = [seis,zeros(nsamp,1000)];
    ibuf = [ibuf,zeros(120,1000)];
    lbuf = [lbuf,zeros( 60,1000)];
  end

%  keyboard
  ibuf(:,nx) = T1;
  lbuf(:,nx) = T2;
  seis(:,nx) = T3;
end

%fprintf(1,'There are %d seismograms of %d points each\n',nx,nsamps);
```

```
fclose(fid);

seis = seis(:,1:nx);

    % 27L - used by UTIG as 4-byte lag value - non standard
 long_ix = [1:7,10:17,19:22];   % As per SEG-Y standard

 % 47 - SEG-Y standard subweathering velocity
 % 50 - source static correction
 % 51 - group static correction
 % 52  - total static correction
 % 53  - lag time A -time difference between source header time and time break
 % 54  - lag time B - time between time break and initiation of source
 % 55  - deep water delay time between energy source and time when recording starts
short_ix = [15:18,35:36,45:59 63:90];  % As per standard

               % Last 60 bytes contain optional entries
aux_short = [ 91:120];
aux_long  = [ 46:60];

header.sactive = intersect(find(any(ibuf,2)),union(short_ix,aux_short));
header.lactive = intersect(find(any(lbuf,2)),union(long_ix,aux_long));
header.short = int16(ibuf(header.sactive,1:nx));
header.long  = int32(lbuf(header.lactive,1:nx));
read_time = toc;

if nx > 1000
  fprintf(1,'Read %d traces in %.3f s\n',nx,read_time);
end
```

butter_filt

```
function  [B,A] = butter_filt(n,fc,dt,type)
% BUTTER_FILT - creates a butterworth lowpass filter coefficients of order n
%
%    [B,A] = butter(filt(n,fc,dt,type)
%
%  n - order of the filter.
%      The drop off of the filter is approximately  6*n dB/octave
%
%  fc - corner frequency(s) of filter.
%  dt - sample rate of data
%
%  type  - 'low', 'high','bandpass'
%
% B,A  - numerator & denominator of IIR filter. To apply filter use the
%        Matlab function
% To apply the filter use the Matlab function filter
%              y = filter(B,A,x)
%
% Implementation based on Wikipedia articles on Butterworth filter & bilinear
% z-transform.
% Though note  bilinear tranform implied here is
```

```
%           s <- 2/dt (1-z)/(1+z)
% As I want stable filter in terms of z not z^(-1)
%
% a. j. harding

fcnorm = fc*dt;

if (n <= 0)
 error('Order of filter (%d) must be > 0',n);
end

if (any(fcnorm < 0) | any(fcnorm >= 0.5))
 error('Corner frequency %.1f outside range [0,fnyq]');
end

if (nargin < 4)
  type = 'low';
end

if ~any(strcmp(type,{'low','high','bandpass'}))
  error('Unrecognized filter type %s',type);
end

nby2 = floor(n/2);

theta = (2*[1:nby2]+n-1)*pi/2/n;   % roots on unit circle

% fa = 1/pi/dt * tan(pi*fcnorm);  % pre-warped corner frequency
av  = 1./tan(pi*fcnorm);    % scaling factor based on corner frequency

if any(strcmp(type,{'low','bandpass'}))
 a = av(end);
 asq  = a*a;
 asqp = asq+1;

 if (mod(n,2) == 1)    % Odd power => pole at -1
   scalef = (1+a);
   B = [1,1];
   A   = [1, (1-a)/scalef];
 else
   scalef = 1.;
   B = 1;
   A  = 1;
 end

        % Add response due to other poles as conjugate pairs for effieciency
        % & to avoid complex coefficients/calculations.
 for k = 1:nby2
   scalep = asqp - 2*a*cos(theta(k));
   B = conv(B,[1,2,1]);
   A     = conv(A,[1,-2*(a^2-1)/scalep, (asqp+2*a*cos(theta(k)))/scalep]);
   scalef = scalef * scalep;
 end;
```

```
 B = B/scalef;

 if strcmp(type,'low')
   return
 else
   Bl = B;
   Al = A;
 end

end

       % Now do high pass end
 a = av(1);
 asq  = a*a;
 asqp = asq+1;

 if (mod(n,2) == 1)    % Odd power => pole at -1
   scalef = (1+a);
   B = a*[1,-1];
   A   = [1, (1-a)/scalef];
 else
   scalef = 1.;
   B = 1;
   A  = 1;
 end

         % Add response due to other poles as conjugate pairs for effieciency
         % & to avoid complex coefficients/calculations.
 for k = 1:nby2
   scalep = asqp - 2*a*cos(theta(k));
   B = asq*conv(B,[1,-2,1]);
   A     = conv(A,[1,-2*(a^2-1)/scalep, (asqp+2*a*cos(theta(k)))/scalep]);
   scalef = scalef * scalep;
 end;

 B = B/scalef;

if strcmp(type,'bandpass')
  B  = conv(B,Bl);
  A  = conv (A,Al);
end
```